Abstract

CURRY, ADAM CRAIG

Methods of measuring flash temperatures in the grinding of MgO-doped PSZ

(Under the direction of Dr. Albert Shih)

This study is based on results of a test to determine mechanisms in the grinding of partially stabilized zirconia. The grinding mechanism tests, which are outlined, suggest involvement of a thermal mechanism, a hypothesis of which is outlined. In order to validate this hypothesis, an investigation of flash grinding temperatures, an indicator of heat generation and thereby a means to validate the hypothesis, was conducted.

The theoretical background, actual implementation, and results of each of three different temperature analysis methods are presented. The first method, a single-wavelength infrared camera, provided indications of temperature distribution. However, it did not provide temperature indications because of uncertainties in the grinding process that make calibrations ambiguous. The second method, a dual-wavelength ratio method, verified the possibility for fast time-response analysis of the grinding process. As an adequate calibration was not achieved for this method, it provides no quantitative results. The third method is the implementation of a spectrometer, which provided repeatable calibrated flash temperature indications. Results from this portion of the study indicate temperatures that, for the range of wheel speeds and downfeed rates tested, depend solely on the wheel and workpiece used. For these tests, dense vitreous bond silicon carbide grinding wheels generate temperatures of 3000 K for grinding MgO-doped zirconia and temperatures of 2400 K for grinding alumina. When grinding these materials with a

diamond abrasive wheel, temperatures of 3000 K for grinding zirconia were registered, and no signal was registered for grinding alumina. Finally, the implications of the results of these various tests are discussed.

METHODS OF MEASURING FLASH TEMPERATURES IN THE GRINDING OF MgO-DOPED PSZ

by
ADAM CRAIG CURRY

A thesis submitted to the Graduate Faculty of
North Carolina State University
in partial fulfillment of the
requirements for the Degree of
Master of Science

MECHANICAL AND AEROSPACE ENGINEERING

Raleigh, NC

2001

APPROVED BY

_____ _____

_____
Chair of Advisory Committee

Dedication

May this work serve to glorify God.

> *For God, who said, "Let light shine out of darkness," made his light shine in our hearts to give us the light of the knowledge of the glory of God in the face of Christ. But we have this treasure in jars of clay to show that this all-surpassing power is from God and not from us.* *2 Corinthians 4: 6-7*

Biography

Adam Curry is the second son of U.S.A.F. Lt. Col. Donald and Laura Curry and the brother of Don Curry Jr.. Although Adam's and Don's parents continue to serve their country in locations around the world, the Curry family considers North Carolina home.

Acknowledgements

Many thanks to:

My parents, Don and Laura Curry, for their unfailing support, encouragement, faith, and prayers.

My brother, Don Curry Jr., for his constant guidance, example, support, and friendship.

Dr. Albert Shih, for his encouragement, direction, time, and energy, which not only made this project possible, but had lasting personal impact.

Chrissy Ficarra, for her unending encouragement, support, and friendship.

Brian Rhoney, for his friendship throughout the past three years.

Dr. Yates Sorrell, for his encouragement and his support in the field of optical temperature measurement.

Dr. Ron Scattergood, for providing his expertise in materials science.

Everyone at Oak Ridge National Lab who assisted in this research, especially:

- Dr. Arvid Pasto, for coordinating the involvement of NCSU with ORNL.
- Dr. Ray Johnson, for his guidance on this project.
- Sam McSpadden, for facilitating the work at Oak Ridge National Laboratory (ORNL).
- Tyler Jenkins, for providing exceptional technical support on this project.
- Dr. Ralph Dinwiddie, for his suggestion of measuring the temperature through the semi-transparent workpiece; conducting the tests with the infrared imaging camera; providing references; and offering infrared measurement equipment.
- Curt Maxey, for assisting in the development of the two-sensor systems; providing optical measurement equipment; and offering optical design expertise.

Everyone at Cummins Diesel Engines who assisted in this research, especially:

- Tom Yonushonis, for his support of this research.
- Darryl Gust, for his guidance on this project.
- Mike Bowling, for his technical support and machine-work

Table of Contents

List of tables

List of figures

1 Introduction

1.1 Importance of temperature-measurement in grinding

Heat generation is a cause of "some of the most serious problems encountered in precision grinding" (Malkin, et al. 1974). It may affect the workpiece and/or grinding wheel. On the wheel, heat may degrade the integrity of the matrix or the abrasive. Excessive temperatures at the workpiece surface reduce surface quality by causing thermal cracks or, in some cases, burning the surface. Thermal gradients introduce strength-reducing tensile residual stresses. Dimensional inaccuracies may result from these gradients. Temperature may also influence the grinding mechanism (Ueda, et al. 1992), either by softening the material or by introducing phase transformations. The introduction of phase transformations due to elevated surface temperatures is the primary thermal effect of present interest.

1.2 Literature review

A number of researchers have undertaken the task of determining the temperatures generated during grinding. Analytical and empirical methods, and combinations of the two, have been employed. Although earliest attempts focused on the grinding of metals, some studies in the past two decades have included ceramics.

A pioneering work was performed by Outwater and Shaw (1952). Their analytical approach, which is based upon Jaeger's classic moving heat source model (Jaeger, 1942), assumes that all grinding energy is taken up in the shearing required for chip formation. Surface temperature is then determined by assuming that a partition of

that energy flows into the chips, and the remainder acts to raise the workpiece surface temperature. For experimental verification, Outwater and Shaw used a toolwork thermocouple technique, in which dissimilar metal wires are smeared across the face of the workpiece to form the hot junction of a thermoelectric circuit. This provides a temperature indication during grinding that is the average temperature across the area formed by the junction of the wires. (Malkin and Anderson, 1974)

1.2.1 Single-wavelength methods

Kops and Shaw (1983) are among the first to use infrared methods in grinding analysis grinding. They used high-speed infrared films, lead sulfide photocells, and digital infrared (IR) imaging cameras to sense aspects of the grinding process occurring outside of the visible light spectrum. Such work provided qualitative information about grinding, but no quantitative temperature indications.

Various researchers have used single-wavelength detectors to measure grinding temperatures. Ueda, et al. (1985) used optical fibers in the collection of infrared radiation from the wheel after it leaves the grinding zone. In their study, a fiber was directed toward the grinding wheel surface at various positions about the periphery of the wheel. The fiber directed the signal to an infrared sensor. A heat transfer analysis provides the temperature at the grinding zone. This method therefore depends on spatial and temporal extrapolations of the data. Such extrapolations may not accurately indicate the highest temperatures generated.

In a study by Ueda, et al. (1992), a similar method is used to determine subsurface temperatures during the grinding of ceramics. In this case, a blind hole was drilled into

the bottom of the workpiece. One end of the fiber, positioned in the hole, collected radiation from the upper surface of this hole, as the grinding wheel passed on the top of the workpiece. Temperature indications were monitored as the thickness of the remaining material decreased. Surface temperatures were provided by extrapolating the temperature trend to a "zero thickness" condition.

Chandrasekar, et al. (1990) conducted measurement studies of infrared radiation emitted in the grinding of metals and magnetic ceramics. Measurements were taken from the wheel as it passed over a 2-mm diameter hole in the workpiece. This radiation was directed to a single-wavelength detector. This technique provides an indication of the temperature rise of the wheel from the grinding process, but does not indicate the flash temperatures generated during grinding.

The single-wavelength methods employed in the above studies rely upon a measurement of emissivity or calibration of the sensor to the measured surface at a series of known temperatures to arrive at a correlation table. Potential problems with such methods are that: 1) the emissivity is assumed to be constant with temperature, which may not be the case, and 2) only one material is assumed to emit for calibration purposes, although multiple materials may emit during the grinding process.

1.2.2 Multiple-wavelength methods

Hebbar, et al. (1992) were among the first to address these issues by using a method which continually compensates for varying emittances. A common multiple-wavelength assumption is that the emissivity of a surface is nearly constant at nearly adjacent wavelengths. Based on this assumption, the voltage output of a detector at one

wavelength is used to normalize the outputs of the others. The resulting ratios directly correspond to the temperature of the source, regardless of its emittance. In their study of the dry grinding of silicon nitride, zirconia, sapphire, and Ni-Zn with diamond abrasives, the infrared emission was measured at three wavelengths. By normalizing the signal at two of the wavelengths to the signal at the other, the temperature was determined directly (this method will be discussed in greater detail in Section 4.2, Optical method theory). As in the work by Chandrasekar, et al. (1990), the radiation was measured through a 2 mm diameter hole in the workpiece. This gives a temperature indication of the wheel just after grinding, but not during the actual grinding process, when generated temperatures may be much higher.

Zhu, et al. (1995) also used a multiple-wavelength method to correct for unknown emittances. In their study of the dry grinding of silicon nitride with diamond abrasive wheels, it was discovered that the results of a two-wavelength method indicated a nearly consistent apparent emittance, which was then used to correct the signal from a single detector. The subsurface temperatures of the workpiece were measured through a blind hole in order to determine the energy partition to the workpiece during the grinding of ceramics.

1.2.3 Sliding temperature methods

Griffioen, et al. (1985) contributed research on a fundamental component of grinding, the temperatures generated at the interface between two objects moving relative to each other. As indicated by Kannappan and Malkin (1972), rubbing temperatures are an important component of grinding surface temperatures. In the study by Griffioen et al.

(1985), a silicon nitride pin was caused to bear, with various loads, upon a sapphire disc spinning at selected speeds. Optical temperature signals generated at the interface, and transmitted through the sapphire disc, were measured with an infrared scanning camera.

Calibration of the camera's output was achieved by heating the pin to a given temperature, as indicated by a thermocouple, and noting the camera's corresponding output voltage. By measuring camera output at a variety of pin temperatures, a correlation table was created. Pin temperatures for calibration were limited to 473 K. Yet tests indicated interface temperatures of up to 2973 K. At such high temperatures, the researchers were forced to rely upon extrapolations of their calibration data. The accuracy of such extrapolations is not known.

Farris and Chandrasekar (1990) measured the temperature generated by a diamond indenter sliding under load on polycrystalline Ni-Zn ferrite and single-crystal sapphire. The temperatures in the ferrite and sapphire were measured through a 2 mm diameter hole. Since sapphire is nearly 90% transparent in the infrared range used, measurements were also made directly through the sapphire workpiece. Emissivities were measured for the diamond, ferrite, and sapphire at various temperatures. Temperatures generated during the test were then correlated to detector output by making emissivity and transmissivity corrections as needed. Results for the temperature through the sapphire were reported to be about 16% higher than the temperature observed through a viewing hole. This finding is potentially significant for the current research, as the temperatures being measured through the workpiece will be compared to the results of researchers who have measured through viewing holes.

1.2.4 Analytical Methods

Most of the aforementioned studies have attempted to correlate experimental results with one or another of the many analytical models that have been devised. This body of strictly analytical work on thermal aspects of grinding has not yet been discussed in this paper. Because of its value in understanding the thermal phenomena associated with grinding and in interpreting the results of the experiments conducted, an overview of this analytical work will be provided. However, as this project is not concerned with the development of analytical models, they will not be treated in detail.

An excellent overview of the analytical work up to 1991 is presented by Lavine (1991). Lavine begins with the work of Outwater and Shaw (1952), which assumed that all grinding energy was applied to the chip formation shear plane. Hahn (1956) contributed a consideration of the energy dissipated as the worn flat area of a grain moves over the workpiece. Des Ruisseaux and Zerkle (1970), Malkin and Anderson (1974), and Malkin (1974) further developed the previous models to determine the workpiece background temperature and the shear plane temperature. Malkin (1974) also determined the temperature from the friction at the worn flat areas of the grits. These models all assume an energy partition to the workpiece. To correct for this uncertainty, Lavine (1988), Lavine and Jen (1991), and Lavine et al. (1989) developed models that include the effects of heat transfer to the wheel grains and grinding fluid. The value of the energy partition to the workpiece therefore need not be specified. However, these models assume that all heat is generated at the abrasive wear flats. Lavine (1991) proposed a model that accounts for heat generation at the shear planes as well.

In a previous study, Malkin (1968) showed that the grinding energy is divided between shearing for chip formation and friction on the grinding surface of abrasive grits that are worn flat. This is evidenced between the correlation between the increase of the sizes of these worn flat areas and the sliding energy in grinding.

Kannappan and Malkin (1972) proposed that the grinding energy is divided among chip formation (which includes shearing energy of the chip and friction of the abrasive against the chip), plowing of the abrasive through the workpiece, and sliding of the worn flat areas against the workpiece.

Jen and Lavine (1995) report on their development of a model that accounts for variation in the heat flux with location in the grinding zone. Their previous models, such as the one reported by Lavine (1991), assume the heat fluxes in the grinding zone are uniformly distributed.

A model developed by Guo and Malkin (1995) dictates that the energy partition varies along the grinding zone, such that the temperature of the wheel and coolant, treated as a thermal composite, match the temperature of the workpiece at every point. Ju, et al. (1998) explain that the model presented by Lavine and Jen is limited to large Peclet numbers and down grinding and proceed to outline their development of a model which alleviates these restrictions.

1.3 Summary of temperature measurement and modeling methods

Based partly upon the work of the researchers above, six possible methods for temperature determination have been outlined. They are:

1) Monitor the incandescent transmission through optically transmitting samples during grinding, and correlate detector output with temperature. This may be done at a single or multiple wavelength(s).
2) Drill a small hole through workpieces to the grinding surface. Monitor the incandescent signal through the hole and correlate it with temperature, as above.
3) Drill a blind hole into workpieces to monitor subsurface temperatures. Approach surface temperature determinations by approaching "zero thickness".
4) Embed thermocouple(s) in workpiece, and monitor temperature at thermocouple as ground surface approaches thermocouple. Extrapolate temperature for when ground surface reaches thermocouple.
5) Calculate expected grinding surface temperature, based on energy partition.
6) Model grinding with CFD (computational fluid dynamics)-capable FEA (finite element analysis) program.

The selection of an appropriate method for the research presented in this report will be explained shortly. In Section 2 of this report, a study on mechanisms of grinding zirconia will be presented. Section 3 is an introduction to thermal considerations in grinding and the thermal hypothesis arising from the study in Section 2. This is followed, in Section 4, by a discussion of the optical temperature measurement methods employed in this study. Finally, Section 5 provides concluding remarks and recommendations for further investigation.

2 Grinding mechanism study on SiC grinding of MgO-PSZ

2.1 History of SiC grinding of zirconia

Dr. Albert Shih and Tom Yonushonis discovered an unusual grinding phenomenon while testing the performance of a variety of vitreous bond SiC wheels on zirconia used for diesel fuel injectors (Shih and Yonushonis, 2000). This began an investigation into the grinding of a Partially Stabilized Zirconia (PSZ) supplied by Coors Ceramics under the name MgO-PSZ (Transformation Toughened Zirconia), with Silicon Carbide (SiC) grinding wheels.

2.2 Importance of SiC grinding of PSZ

Partially Stabilized Zirconia (PSZ) has been applied extensively in diesel engine fuel system plunger applications [Mandler et al., 1997]. Tightening diesel exhaust emission regulations set by the Environmental Protection Agency in the past two decades have created the need to increase fuel injection pressure and reduce the sulfur content of diesel fuels. Closely matching the plunger and barrel dimensions to sub-μm precision is necessary to generate high injection pressures and the resulting increase in combustion performance.

The low lubricity of low-sulfur fuels tends to cause fuel plunger seizure in close-tolerance plunger designs. However, the use of PSZ as a plunger material alleviates this problem because of zirconia's low friction coefficient. Furthermore, the thermal expansion coefficient of PSZ closely matches that of steel, which ensure the clearance between the barrel and plunger will be maintained over a wide temperature range. Other

characteristics of PSZ that make it suitable for plunger applications include the high fracture toughness, low wear rate, and low density.

Machining cost is another critical material selection criterion for plunger applications. As the shapes of plungers for diesel fuel systems become more complicated, the machining costs tend to increase. One effective, but still in general costly, method is to generate the negative of the desired form on the grinding wheel. The wheel itself must therefore be machined. Not only the cost of the grinding wheel, but the cost to machine it, are of concern. SiC wheels excel in both of these areas. While diamond for machining typically costs about $3250/kg, and CBN costs about $6700/kg, SiC costs only $1.87/kg, in green form. (Gary, 1999). Furthermore, SiC wheels are much easier than diamond or CBN to machine to various desired geometries.

While SiC shows many potential advantages, the accepted practice in grinding is to use a grinding wheel of material with hardness much greater than that of the material to be ground. For grinding materials such as PSZ, this typically means grinding with

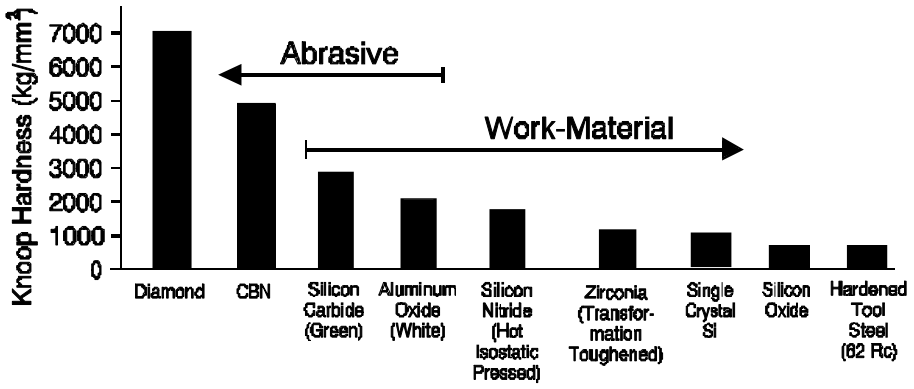

Figure 2.1: Grinding material hardnesses

diamond or cubic boric nitride (CBN). The amount of ground material wear versus grinding wheel wear (quantified as the G-ratio) for these materials is high. Although SiC is not expected to generates such high G-ratios, its clear material and machining cost advantages may make it the most economical choice.

$$G-ratio = \frac{volume\ of\ workpiece\ material\ removal}{volume\ of\ wheel\ wear} \tag{2.1}$$

Tests of grinding MgO-PSZ with certain wheels of SiC reveal unexpectedly high G-ratios. In initial tests on a Studer cylindrical grinder, ratios of over 800 were achieved. Such high G-ratios, combined with the low material and machining costs of SiC, make it a promising choice for grinding MgO-PSZ. However, the implications of this discovery have not yet been fully explored. To understand and exploit the grinding mechanisms at work, an investigation of the behaviors of various ceramics, ground over a range of downfeed rates and table speeds, was arranged.

2.3 Grinding mechanism study

Various features and grinding effects were observed in the course of this investigation. For each area of investigation, the downfeed, wheel speed, and grinding table speed were recorded. The resulting G-ratio for each was determined. Because of the significance of transformation toughening in the workpiece, the effect of grinding on the phases present was one of the primary areas of investigation. The remaining were surface topography (as viewed by scanning electron microscopy, or SEM) and temperature at the grinding surface. Each of these areas of investigation will be addressed in turn.

2.3.1 Experiment design

For further investigation into the grinding mechanisms involved, surface, rather than cylindrical, grinding was chosen. Because surface ground parts are flat, material analysis is easier than on cylindrically ground parts. The various effects (surface topography, G-ratio, and phase analysis) mentioned above were measured for each entry in a matrix of grinding tests. On each of two grinding machines, the following parameters were varied: grinding table speed, or the speed of the part to be ground as it is drawn across the wheel; down-feed, which is the amount by which the grinding wheel is advanced into the part with each pass; and grinding method, which refers to the direction of the grinding wheel. As shown in Figure 2.2, if the direction of wheel rotation is such that it tends to pull the part up from the table, the method is considered up-grinding. If the wheel tends to push the part down onto the table, it is considered down-grinding.

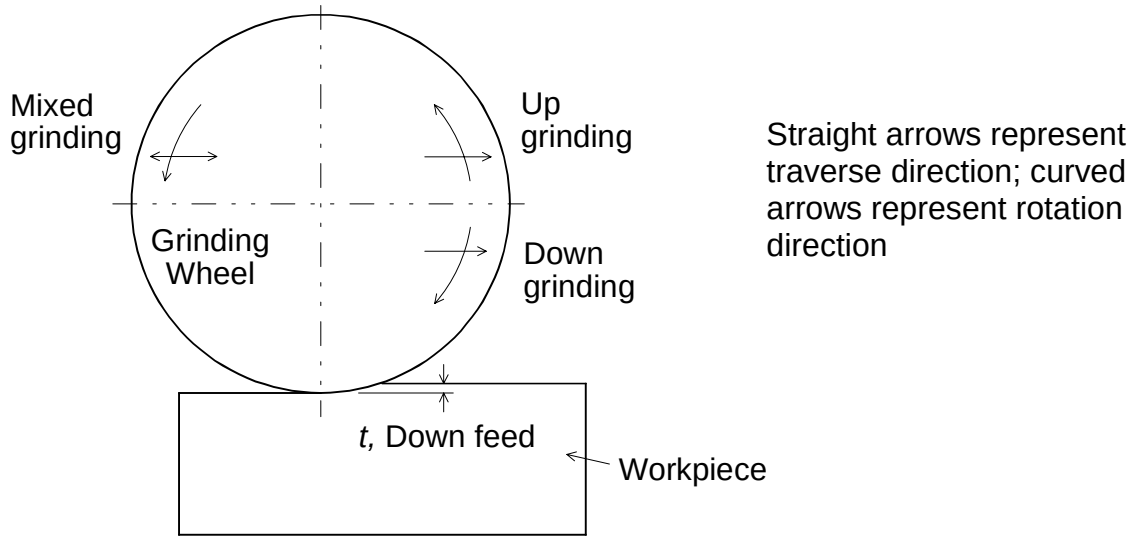

Figure 2.2: Grinding parameters

The machines, one a Nicco and the other a Harig, exhibit different stiffness values and motor power ratings. The Harig is best suited for shallow-cut grinding, while the Nicco is capable of the large depths of cut associated with creep grinding. The Harig is a lower cost machine with 6140 N/mm structural stiffness, versus the Nicco's 15600 N/mm. The Harig machine accommodates fast table speeds, but the down feed rate is limited. In contrast, the table speed in the Nicco is limited while large down feed rates are typically used. The Harig has a relatively small, 1.12 kW spindle motor relative to the Nicco's 5.6 kW. Due to their different performance characteristics, the grinding method used depended on the machine. On the Harig, up-grinding was the standard. On the Nicco, down-grinding was the standard. Together, these two machines provided a variety of grinding conditions.

Four table speeds, 50.8, 112, 173, and 229 mm/s, were used in the Harig. Five much slower table speeds, 0.42, 1.69, 2.54, 3.39 and 6.77 mm/s, were used in the Nicco. Three down feeds, 0.0025, 0.005, and 0.013 mm, were used in Harig. The corresponding specific material removal rates for the 12 grinding tests in Harig are shown in Table 2.1. In the Nicco grinder, five down feeds, 0.635, 1.270, 1.905, 2.540, and 3.175 mm, were used. These values were chosen such that the specific material removal rates of the 15 grinding tests in the Nicco match those in the Harig.

The material used in the baseline grinding tests was Coors MgO-PSZ (Transformation Toughened Zirconia), a MgO-doped PSZ. Other ceramics studied include Coors YTZP ,an yttria-doped PSZ; AD-94, 94% alumina; ZDY, an yttria-doped

fully stabilized zirconia. Only selected grinding tests, rather than the full scale of 27 tests listed in Table 2.1, were performed on the YTZP, AD-94, and ZDY.

All other grinding parameters remained constant during the tests. The coolant used was water-based Cimtech 500 synthetic coolant at 5% concentration. The wheel speed was 3700 rpm or 37.2 m/s surface speed.

Table 2.1: Specific material removal rates

Specific material removal rate, $mm^3/sec/mm$									
Harig				Nicco					
Table speed	Down feed (mm)			Table speed	Down feed (mm)				
(mm/s)	0.0025	0.005	0.0127	(mm/s)	0.635	1.27	1.91	2.54	3.18
50.8	0.13	0.26	0.65	0.42	0.27	0.54	0.81	1.08	1.34
112	0.28	0.57	1.42	1.69	1.07	2.15	3.23	4.30	
173	0.44	0.88	2.19	2.54	1.61	3.23	4.84		
229	0.58	1.16	2.90	3.39	2.15	4.30			
				6.77	4.30				

Grinding wheel and wheel dressing

For each grinding test, a dense vitreous bond SiC grinding wheel, provided by Norton Corp., was used. Each wheel was trued with a Winter flissen diamond truing tool DT 0699 FDS-75-H at 254 mm per minute cross-feed rate and 2.54 micrometer depth of material removal. The wheel is 12.7 mm wide and, after truing, is 200 mm in diameter.

The diamond wheel was trued with an electric truing motor, using a SiC or diamond truing wheel.

Grinding fixture

A special fixture was designed and constructed by Mike Bowling, of Cummins, for clamping samples to the table during grinding. The fixture holds from one to five tiles securely, and since only a small amount of tile is held by the fixture, it allows most of the tile to be ground for the tests.

Force and power measurements

Forces in the three coordinate directions (up/down, left/right, in/out) of the table were measured with a piezoelectric Kistler dynamometer attached to the table and monitored by a personal computer on LabView data analysis software. Force measurements were taken over the initial and final 30 seconds of each grinding test. Power consumption was monitored over the same periods.

Swarf

For each grinding test entry on the Harig, the grinding debris, or swarf, was collected for analysis as well. Each method collects the coolant in which the swarf becomes trapped during grinding. For the swarf collection part of each test, the grinding machine coolant system was disconnected. A bucket of clean coolant was placed above the coolant outlet at the wheel and routed through a plastic tube, to provide a gravity-fed supply of coolant. For this arrangement, all coolant was collected; none was reused.

a) Fixture and ceramic workpieces

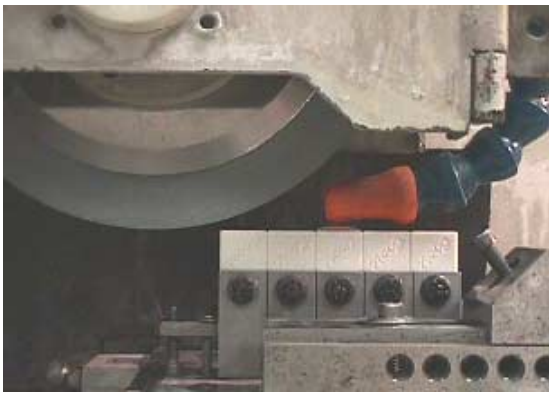

b) Wheel, workpieces, and coolant nozzle

c) Truing the SiC wheel

d) Nicco and data acquisition system

Figure 2.3: Grinding test arrangement

2.3.2 G-ratio

To determine the G-ratio for each test, the change in height (and thereby volume) of the ceramic tile was measured, as well as the depth of the groove (and thereby volume) worn into the grinding wheel. The tile height change measurements were made with a micrometer. To measure the depth of the groove worn into the wheel, the form of the groove in the wheel was ground into a soft machinable plastic wear block. The resulting

profile was then measured with a coordinate measuring machine (CMM). The wear volume calculations were entered into Eq. 1 above to determine the G-ratio.

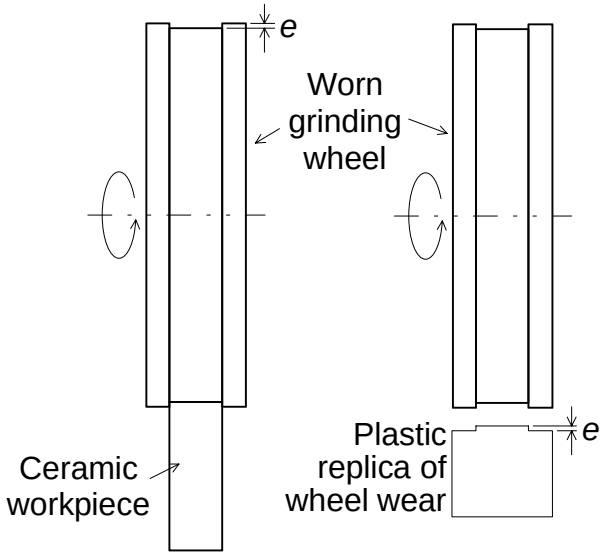

Figure 2.4: G-ratio measurement method

Results of G-ratio measurements for the baseline tests are shown in Table 2.2 and Figure 2.5. Relatively high G-ratios (over 100) can be achieved on the low-stiffness Harig machine. This illustrates the effectiveness of the low cost SiC wheel for form grinding of PSZ. It may be observed that, at the same down-feed rate, a higher table speed increases the specific material removal rate and improves the G-ratio on the Harig machine. The opposite trend can be seen on the Nicco.

At the same specific material removal rate, the G-ratio on the Harig is in general higher that on the Nicco, which has a higher stiffness and was therefore expected to have lower wheel wear. However, this can be explained by the different grinding

configurations used in the Harig and Nicco. Creep-feed grinding is the method used in the Nicco grinder. Usually, very porous vitreous bond wheels are used in creep feed grinding to avoid the loading of debris in the wheel surface pores. The dense vitreous bond SiC wheel has lower porosity and is therefore not ideal for the high down feed, slow table speed grinding. The G-ratio results verify this.

Table 2.2: G-ratio results for baseline tests

G-ratio									
Harig				Nicco					
Table speed	Down feed (mm)			Table speed	Down feed (mm)				
(mm/s)	0.0025	0.005	0.0127	(mm/s)	0.635	1.27	1.91	2.54	3.18
50.8	65	56	55	0.42	46	55	62	75	92
112	68	58	65	1.69	45	51	53	64	
173	97	81	59	2.54	36	34	36		
229	113	89	65	3.39	29	30			
				6.77	19				

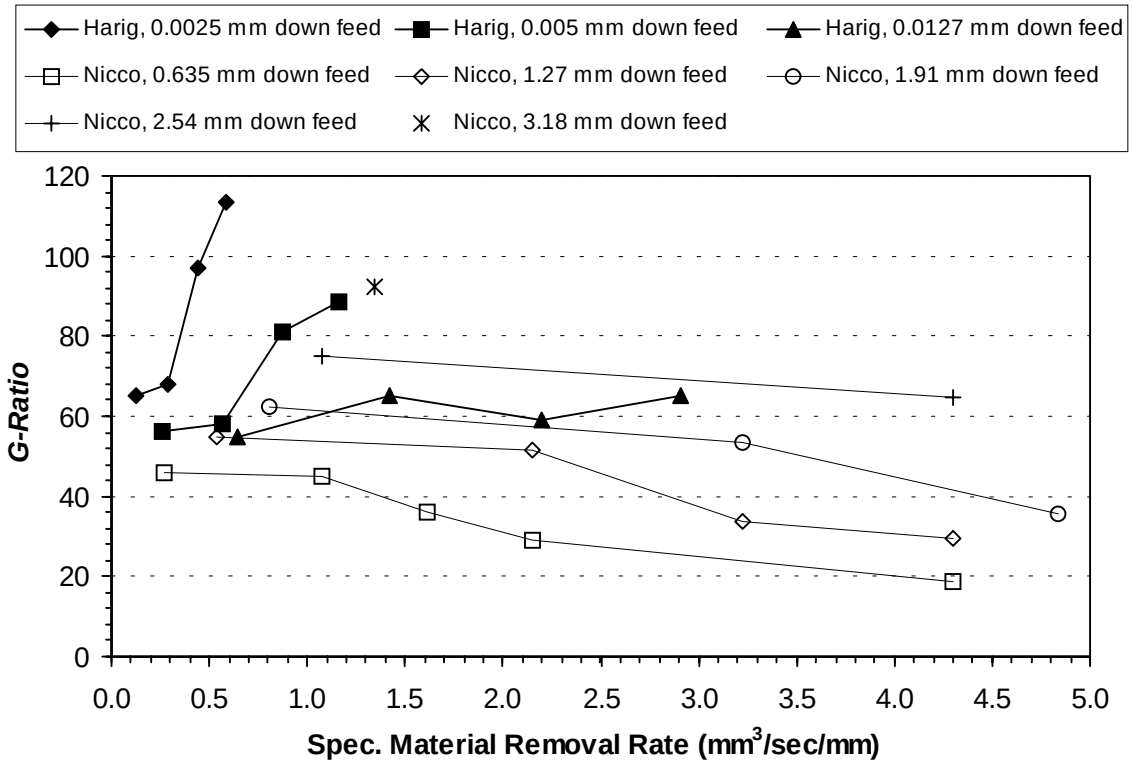

Figure 2.5: G-ratios results of baseline tests

2.3.3 Surface finish

The surface finish along the grinding direction on ground surfaces was measured using a Rank Form Talysurf profiler. The middle three of the five samples in the fixture were measured. The average of the R_a values for the three parts was used to represent the surface finish of each grinding process.

The figure below shows the surface finish results for grinding MgO-PSZ with SiC on the Harig. The high, 0.0125 mm, down feed grinding generates relatively rough surface finishes of about 0.6 to 0.7 μm R_a. Better surface finish, in the 0.3 to 0.4 μm R_a range, is seen at lower down feed rates.

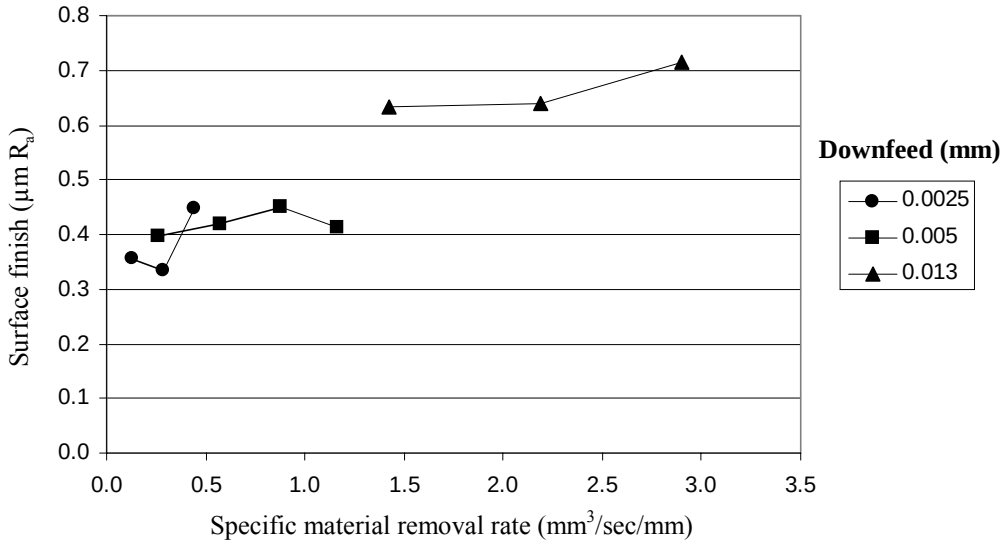

Figure 2.6: Surface finish results

2.3.4 Phase analysis

A room temperature x-ray diffraction machine at Oak Ridge National Lab was used to characterize the phase compositions of the unground ceramic tile surface, ground tile surfaces, and grinding debris.

Samples of ground ceramic and swarf were obtained from each grinding test. X-ray diffraction was performed to obtain a diffraction pattern for each sample. For three groups of 5 ground surface samples, each sample was analyzed, and it was observed that the first sample generally contains a larger percentage of the monoclinic phase than do the other four, which are about equal to each other. Based upon this finding, the third sample from each test was considered for comparison.

Ground and un-ground surface samples were mounted to an x-ray diffraction sample mount using modeling clay, with the ground surface of the sample irradiated. The grinding swarf was gathered by trapping the coolant, in which the swarf was suspended. The swarf was separated from the coolant for analysis. The separated swarf was allowed to dry, then mounted on a single crystal slide by suspending it in a small amount of acetone, which dried to leave the sample affixed to the slide.

The diffraction patterns were used to determine the appropriate PDF cards. Each pattern was compared to the appropriate PDF cards to determine the phases present. This required determining the areas under the relevant peaks to determine the amount of each phase. (The XRD analysis program DMS was used in this study to determine the areas under the peaks.)

The equation below, previously used in studies by Garvie, et al. (1972), Taylor, et al. (1992), and Konsztowicz, et al.(1995), was used to determine the percent of monoclinic phase in each sample.

$$x_m = \frac{I_m(111) + I_m(11\bar{1})}{I_m(111) + I_m(11\bar{1}) + I_c(111)} \tag{2}$$

where I_m refers to the intensities (as indicated by the areas under the peaks representing each plane) of the (1 1 1) and (1 1 –1) monoclinic planes, and I_c refers to the intensity of the (1 1 1) cubic plane.

X-ray diffraction results indicates that the composition of an un-machined part is 9.9% to 10.7% monoclinic phase, for unpolished and polished surfaces, respectively. When other measurements are compared to this baseline, it is found that the amount of monoclinic phase on the ground surface increases, while the amount in the ground debris is negligible. The change of monoclinic phase indicates the degree of phase transformation induced by the grinding process.

Table 2.3: Unground surface phase compositions

Percentage of Monoclinic Phase on the Unground MgO-PSZ Surface

Material	*Surface Preparation*	*% Monoclinic*	*Notes*
MgO-PSZ	Polished	10.7%	Av'g. of 5 scans, each at diff't orient'n
MgO-PSZ	Unpolished	9.9%	1 scan
YTZP	Unpolished	10.9%	1 scan

Table 2.4: Ground surface phase compositions

Percentage of Monoclinic Phase on the SiC Ground MgO-PSZ Surface

	Harig				Nicco				
	Downfeed, mm				Downfeed, mm				
Table speed, mm/s	0.0025	0.005	0.0127	Table speed, mm/s	0.635	1.27	1.91	2.54	3.18
50.8	19.9%	18.4%	16.1%	0.42	13.67%	14.41%	14.59%	11.15%	12.02%
112	20.0%	17.9%	17.2%	1.69	14.36%	15.05%	15.60%	13.96%	
173	19.0%	21.0%	17.0%	2.54	14.69%	13.56%	12.11%		
229	17.0%	19.6%	16.8%	3.39	15.12%	14.07%			
				6.77	15.35%				

Table 2.5: Swarf phase compositions

Percentage of Monoclinic Phase on the MgO-PSZ Grinding Debris

	SiC Wheel			Diamond Wheel		
	Downfeed, mm			Downfeed, mm		
Table Speed, mm/s	0.0025	0.005	0.0127	0.0025	0.005	0.0127
50.8	~0%	~0%	~0%	~0%	5.5%	5.8%
229	~0%	~0%	~0%	5.4%	5.9%	4.8%

2.3.5 SEM Analysis

A Hitachi S-4700 scanning electron microscope (SEM) was used to view and characterize the surface of ground and un-ground ceramic tiles, as well as grinding swarf. Micrographs of the un-ground surface show grain boundaries and reveal that the samples, as supplied, have not been machined.

Ground Surface

Figures 2.7 (a), (b), and (c) show three SEM micrographs of the surface ground at three down feeds and the lowest table speed, 50.8 mm/s. The surface ground with the lowest material removal rate, i.e., 0.0025 mm down feed and 50.8 mm/s table speed, is shown in Fig. 2.7(a). The surface is very smooth, with about 0.35 μm R_a, and free of cracks and surface damage. The porosity of the unground MgO-doped PSZ is visible. At 0.005 mm down feed, as shown in Fig. 2.7(b), some lateral cracks on the surface are seen. At 0.0125 mm down feed, as shown in Fig. 2.7(c), damage on the surface becomes very apparent.

SEM micrographs of three surfaces ground at the highest table speed, 229 mm/s, and three different down feeds are shown in Figs. 2.7 (d), (e), and (f). At 0.0025 and 0.005 mm down feeds, the ground surfaces still show lateral cracking. However, at 0.0125 mm down feed (i.e., the highest material removal rate on the Harig), the lateral cracks are absent. The absence of surface and sub-surface damage is also seen on high infeed rate cylindrically-ground PSZ.

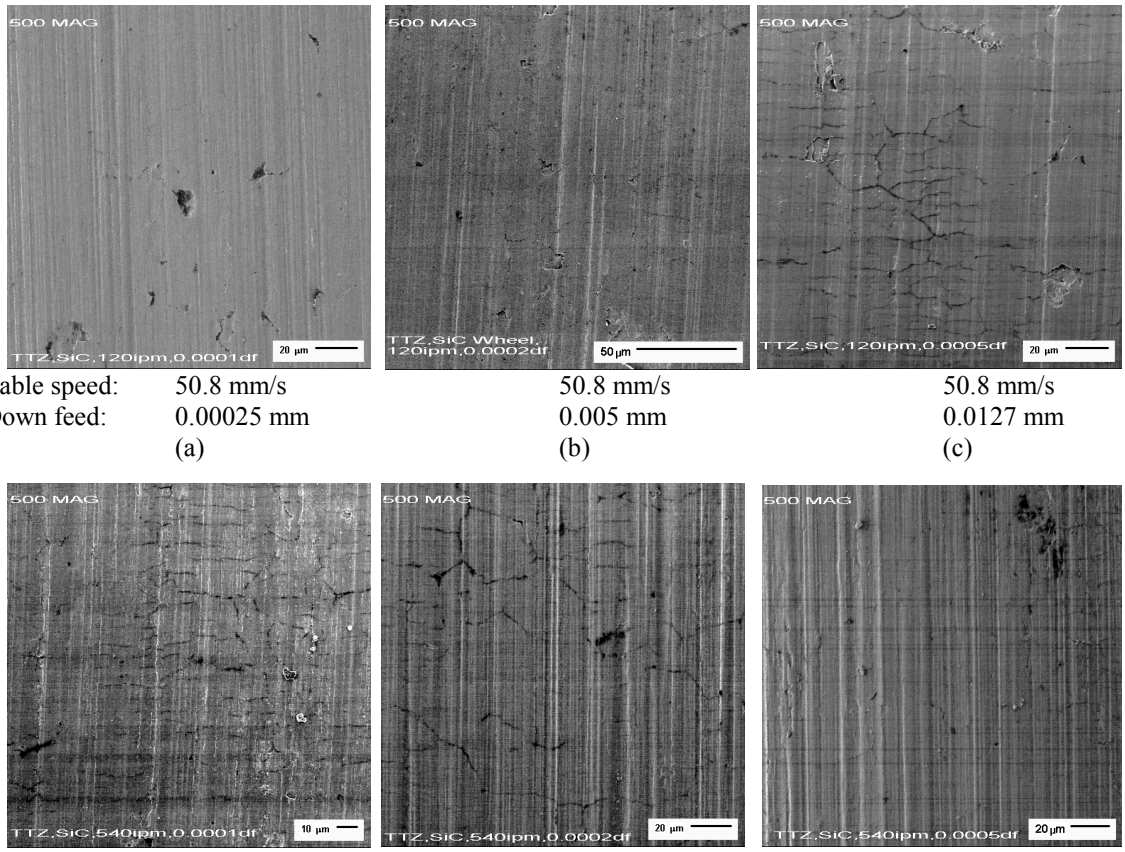

Table speed:	50.8 mm/s	50.8 mm/s	50.8 mm/s
Down feed:	0.00025 mm	0.005 mm	0.0127 mm
	(a)	(b)	(c)
Table speed:	229 mm/s	229 mm/s	229 mm/s
Down feed:	0.00025 mm	0.005 mm	0.0127 mm
	(d)	(e)	(f)

Figure 2.7 SEM micrographs of SiC ground surfaces of MgO-doped PSZ

For comparison with the SiC-ground surfaces, SEM micrographs of MgO-doped PSZ surfaces ground by a 150 grit vitreous bond diamond wheel in the Harig machine are shown in Figure 2.8. Figures 2.8 (a), (b), and (c) show the diamond ground surfaces corresponding to process parameters used in Figs. 2.7(a), (c), and (f). All diamond

ground surfaces are free of lateral cracks, indicating different grinding behavior in SiC and diamond grinding.

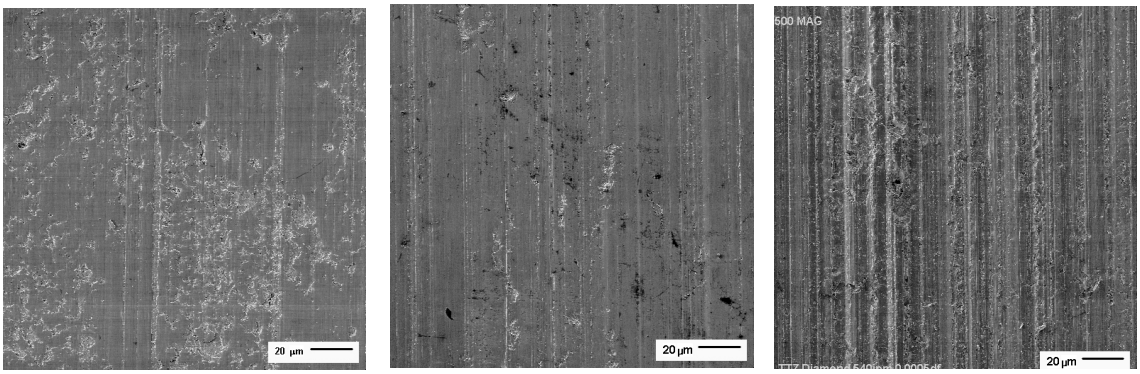

Table speed:	50.8 mm/s	50.8 mm/s	229 mm/s
Down feed:	0.00025 mm	0.0125 mm	0.0127 mm
	(a)	(b)	(c)

Figure 2.8: SEM micrographs of diamond-ground surfaces of MgO-doped PSZ

Debris

Debris of MgO-doped PSZ ground with a dense bond SiC wheel are shown in Figure 2.8. The SEM micrographs show the debris from the six sets of process parameters in Figure 2.7. The debris for all six grinding conditions is small, ranging from 2 to 5 µm. However, agglomeration of debris is a problem that has created difficulty in identifying individual particles of debris.

At the smallest down feed and lowest table speed, as shown in Fig. 2.9(a), the debris shows a flat surface on one side and segregated surface on the other. It resembles a metal cutting chip, which suggests the "ductile regime" grinding mechanism (Bifano, et al. 1991), in which brittle materials behave like ductile metals in machining at low depths of cut. None of the micrographs from the other grinding conditions show similar chip

formation. In these figures, the debris surface is rougher, suggesting a different grinding mechanism.

Figure 2.10 shows SEM micrographs of debris generated using the diamond wheel. The three sets of process parameters are the same as those in Fig. 2.8. Small particles, about 1 μm in size, can be seen for all three grinding conditions. The long debris in Figs. 2.10 (b) and 2.10 (c) indicates ductile regime grinding for these diamond grinding conditions.

While the micrographs are not conclusive, they do suggest a different grinding mechanism at work in the SiC-, versus the diamond-, grinding of MgO-doped PSZ.

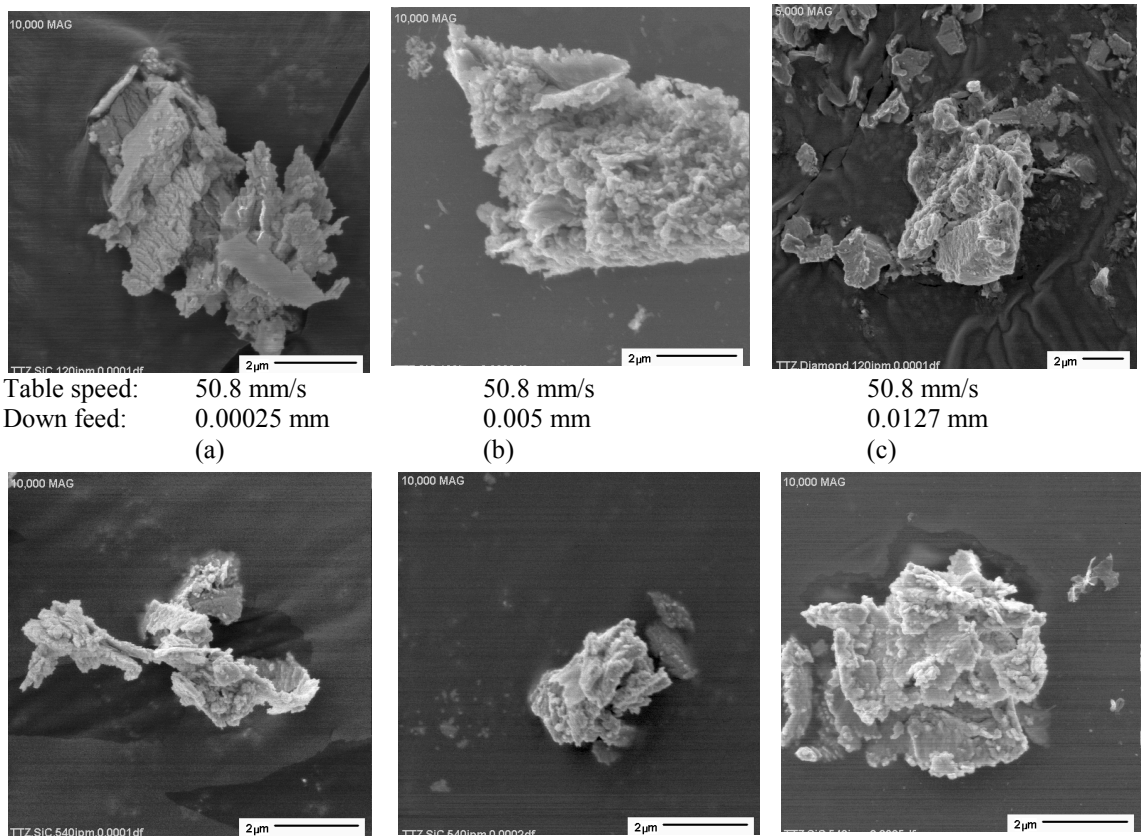

Table speed:	50.8 mm/s	50.8 mm/s	50.8 mm/s
Down feed:	0.00025 mm	0.005 mm	0.0127 mm
	(a)	(b)	(c)
Table speed:	229 mm/s	229 mm/s	229 mm/s
Down feed:	0.00025 mm	0.005 mm	0.0127 mm
	(d)	(e)	(f)

Figure 2.9: SEM micrographs of debris of SiC-ground MgO-doped PSZ

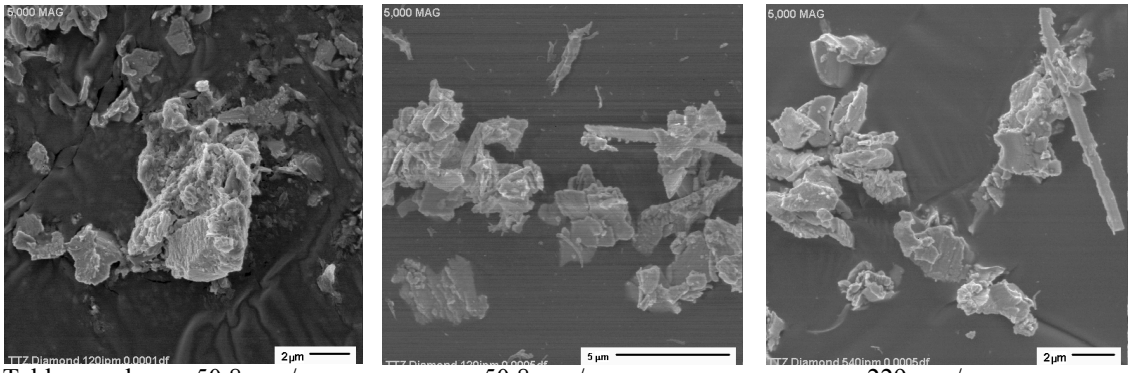

Table speed:	50.8 mm/s	50.8 mm/s	229 mm/s
Down feed:	0.00025 mm	0.0125 mm	0.0127 mm
	(a)	(b)	(c)

Figure 2.10: SEM micrographs of debris of diamond-ground MgO-doped PSZ

3 Thermal effects in grinding

The results of the preliminary investigation outlined above indicate a strong possibility for heat-related effects on the workpiece. The role of thermal effects in grinding, PSZ's phase-temperature relationship, a thermal explanation for the observed behaviors, and a discussion of other researchers' concurrent work are presented in this section.

3.1 Mechanisms of heat generation in grinding

The grinding process is best understood by considering its global and local scales. Grinding performance is discussed in terms such as grinding ratio, ground surface finish, etc.. Of course, such global performance indications are the result of local interactions of individual grits with the workpiece. Indicators of grinding performance include material properties such as abrasive hardness, abrasive friability (tendency to break), and bond stiffness, which are relatively consistent throughout a grinding wheel. Also significant on the local level are geometric properties, such as a grit's wear flat area and rake angle. These factors, which vary significantly among grits, determine each grit's effect on the workpiece. The local and global views of the grinding process provide important insights into the value of a given set of wheel, workpiece, and grinding parameters.

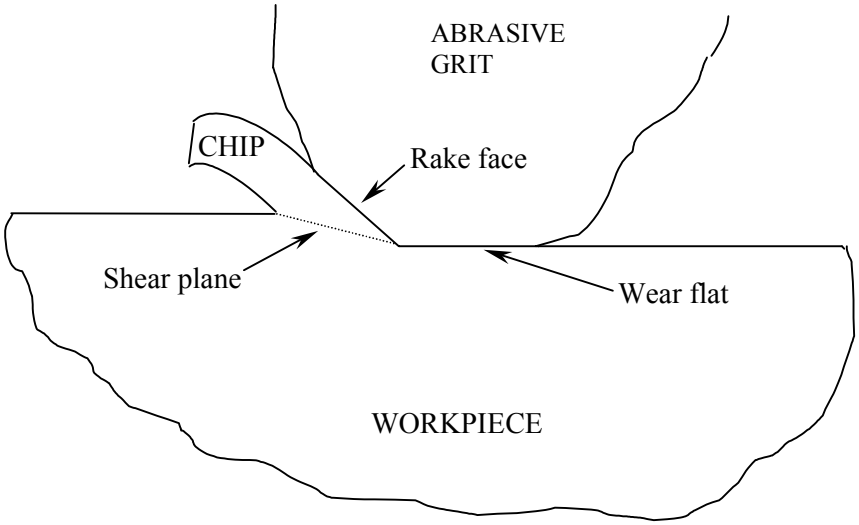

Figure 3.1: Heat generation zones in grinding

Distinctions between global and local effects are particularly important in discussing grinding temperature. As each grain engages the workpiece, it first causes deformation. This stage is known as plowing. If the stress level becomes great enough, chip formation begins. Finally, the chip breaks loose and is carried out of the grinding zone by grinding fluid. The fluid serves both to remove chips, collectively known as swarf, and to cool the workpiece.

Cooling is often critical in grinding because a significant amount of heat is typically generated in the process. Heat is generated primarily by three actions. First is the shearing of the workpiece during chip formation. Second is the friction of the chip sliding at the grit's rake face. Lastly, heat is generated along the portion of the grit worn flat either by truing or by previous passes through the workpiece. Heat generated by any of these means, when it is localized near the grit, is known as flash temperature.

Each grit may be understood as an asperity heat source, with conduction serving to distribute the heat from individual grits and raise the overall temperature of the grinding surface. The temperature far from a grit is known as the background temperature. As would be expected, and as some researchers have shown, the values of these temperatures typically differ significantly, especially in materials with low thermal conductivity, such as ceramics.

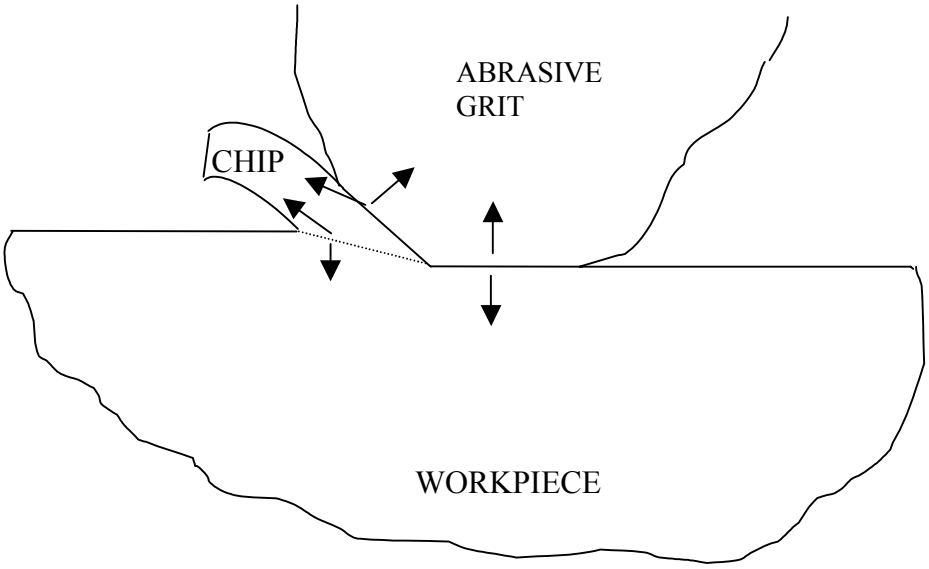

Figure 3.2: Heat fluxes in grinding

The conduction and convection of heat from each heat generation zone (shear plane, wear flat area, and rake face) is often addressed in temperature studies. This heat is apportioned among the chip and coolant, the grinding wheel, and the workpiece. The fraction of heat entering the workpiece is often sought in such studies, since temperature effects on the workpiece are of primary importance. The temperatures measured in this

study, however, are expected to indicate flash temperatures, rather than the distribution of this temperature among its various destinations.

3.2 Material structures of MgO-PSZ

The defining characteristic of transformation toughened ceramics, such as stabilized zirconias (including MgO-PSZ), is their phase composition. Typical ceramics, while demonstrating desirable hardness and wear characteristics, are limited by their brittleness. With the addition of doping agents (magnesium oxide, i.e. MgO, for the MgO-PSZ used in preliminary studies), ceramics can be transformation toughened. The "transformation"

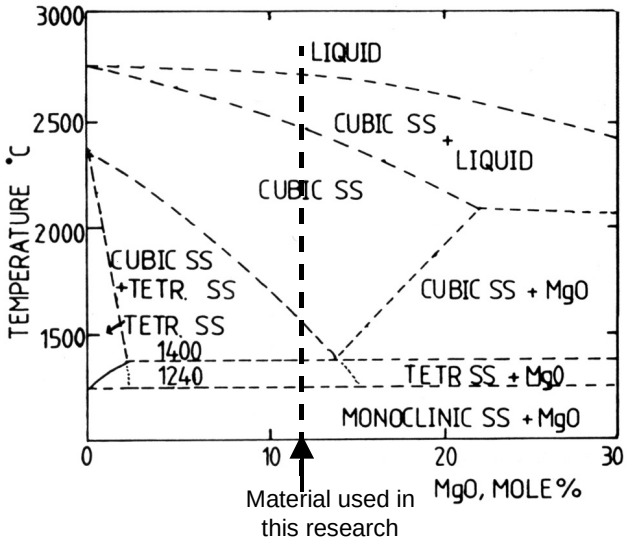

Figure 3.3: Equilibrium phase diagram for ZrO_2-MgO

Ref.: Stevens (1986)

refers to a change of crystal structure, or the arrangement of the molecules in the material. In the case of MgO-PSZ doped with 12% (by volume) MgO, the molecules

may arrange themselves in tetragonal, monoclinic, and/or cubic structures. When the crystal structure is allowed to form uninhibited, the phase observed will depend on the temperature of the ceramic. By quenching (rapidly reducing temperature through immersion in a medium of low temperature), however, the material will be observed to have retained some of the phase from the higher temperature. Therefore, tetragonal and/or cubic phases may be observed in 12% MgO-doped MgO-PSZ at room temperature. Due to the increased size of the monoclinic volume cell, relative to the tetragonal cell, this phase transformation increases the toughness (i.e., reduces the brittleness) of the ceramic (Costa, et al. 1997, and Swain and Hannink 1989).

3.3 Thermal hypothesis

It is proposed that, as compared with grinding by diamond abrasive wheels, more of the heat generated in the grinding of MgO-PSZ with a dense-bond SiC wheel is retained in

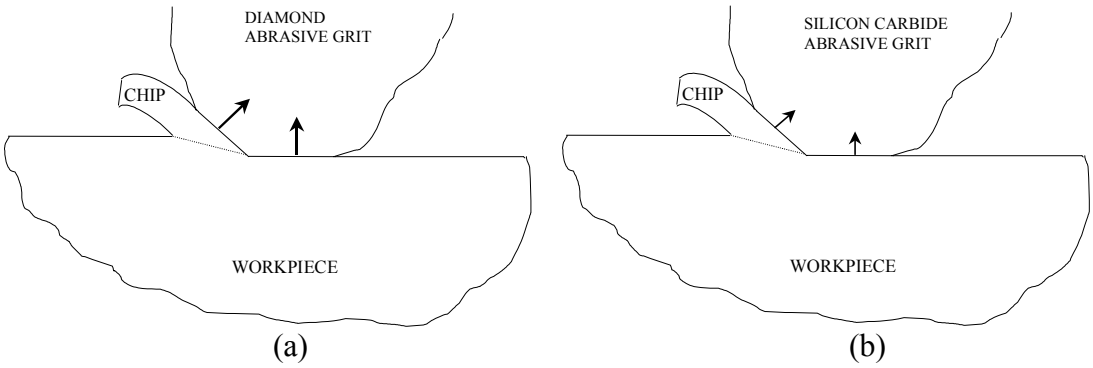

Figure 3.4: Relavtive heat fluxes in diamond versus silicon carbide grinding

the grinding zone. This promotes a higher workpiece temperature. However, due to the low thermal conductivity of zirconia, only a shallow depth into the workpiece reaches a high temperature. Most of the volume of the small zirconia chips does reach the high temperature. The presence of very high temperatures may contribute to an as-yet undetermined phase transformation that assists in grinding. Such a hypothesis explains a number of the observed phenomenon, which are discussed below.

First, the absence of the monoclinic phase in the grinding swarf suggests that its temperature has been raised above the phase transformation temperature to the tetragonal phase (1513 K), then quickly quenched. This is to be expected if the grinding surface exceeds this temperature. Due to their small size, the temperatures of the swarf particles would rise quickly in the presence of a high surface temperature, then cool rapidly as they leave the grinding zone in the cooling fluid. Such a quenching effect would allow the swarf to retain the tetragonal phase, as the x-ray diffraction results indicate.

Second, the increase of monoclinic phase on the surface reflects its exposure to large stresses. However, unlike the swarf, its volume presumably is too large for the temperature of a significant volume to be raised above the phase transformation temperature. Therefore, it does not undergo the phase transformation observed in the swarf, and a large amount of the monoclinic structure is observed on the ground surface.

Third, the reduction of monoclinic phase in diamond-ground swarf, as opposed to its complete exclusion as in grinding with SiC, suggests that the diamond wheel may conduct more of the heat away from the grinding zone. This is likely due to the fact that the thermal conductivity of diamond is an order of magnitude greater than that of silicon

carbide. The surface temperature in diamond wheel grinding apparently still exceeds the phase transformation temperature in some regions, as evidenced by the

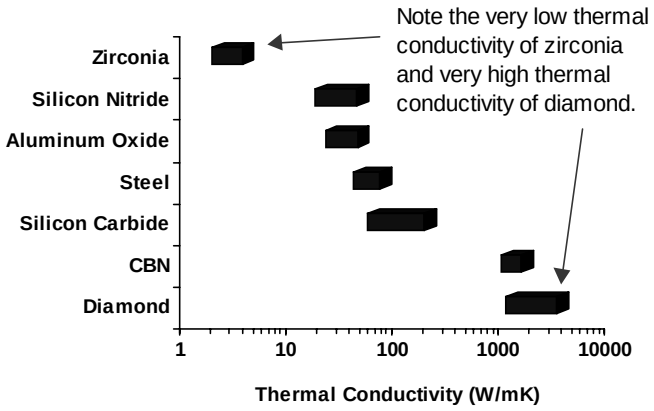

Figure 3.5: Thermal conductivities of various grinding materials

reduction in monoclinic phase in the swarf. However, some of the particles may be larger due to diamond's superior grinding ability. This is supported by the observation of 0% monoclinic in the swarf when using the smallest downfeed rate for diamond grinding of zirconia. As the previous debris particle size analysis did not consider the sizes of diamond-ground particles, further testing is needed to verify that the diamond ground particles are larger.

Together, these results from the preliminary investigation provide a strong indication that high temperatures are a factor in the unexpectedly good grinding performance of a dense vitreous bond silicon carbide wheel on partially stabilized zirconia.

3.4 Concurrent research supporting thermal hypothesis

Two significant studies support this thermal hypothesis. In their studies of abrasive behavior of zirconias, Costa et al. (1997), and Swain and Hannink (1989, Part 2) report that the temperature generated during abrasive processes may counteract the stress-induced transformation (tetragonal to monoclinic) by producing the reverse transformation (monoclinic to tetragonal). That is, temperatures may be reached that elevate the material into the tetragonal phase region, as proposed in this study. Furthermore, Swain and Hannink (1989, Part 2) note that the temperatures at the interface in grinding are expected to be elevated due to the poor thermal conductivity of zirconia. The influence of low thermal conductivities on surface temperatures is an important part of the thermal hypothesis.

As explained previously, for this study it is proposed that the temperature generated in grinding is sufficiently high for the material to enter the tetragonal phase region. The research referenced above supports such a hypothesis. Once it has been established that high temperatures are generated, conduction effects become significant. In regards to this, silicon carbide's and zirconia's low thermal conductivities may trap more heat near the surface than diamond, which is an excellent conductor. Zirconia's tendency to increase surface temperatures is supported by the researchers above; the reduced conductivity of silicon carbide, as compared with diamond, will have the same effect. While the low conductivity of the workpiece likely prevents its surface temperature from rising significantly, the small size of the grinding chips presents less of a barrier to conduction. Therefore, the chip temperature may be elevated to the necessary

phase transformation temperature. Quenching in the cooling fluid would then produce the phase compositions observed.

3.5 Role of temperature measurement in verifying thermal hypothesis

The thermal hypothesis pertains to the heat distribution among the workpiece, wheel, grinding fluid, and surroundings. It is primarily concerned not with the heat generated during grinding, but with how much of the generated heat enters the workpiece and with the spatial variation of the workpiece's resulting temperature.

Methods may be developed to gain such an understanding through direct measurement. However, the simplest initial consideration is the maximum temperature generated by the process. This provides a good indication of whether any volume of the workpiece is exposed to the temperature of concern, whether that be a phase transition temperature, a melting temperature, or some other. Since the maximum temperature is generated at the interface between the wheel and workpiece, in the grinding zone, a determination of this temperature is the first objective.

4 Optical temperature measurement study

For a number of reasons, optical means of determining grinding temperature have been used in this study. The reasons for this choice, the theory behind optical methods, the test arrangements used, the test results, and the implications of those results are discussed in the rest of this section.

4.1 Advantages of optical methods

Although thermocouples are an ideal temperature measurement device for many applications, they are severely limited in measuring flash grinding temperatures. Their shortcomings lie in their poor spatial and temporal resolutions. Spatial resolution is dictated by the size of the hot junction, time response of the thermocouple, and the conductivity through the workpiece. Consider a typical 200 mm diamond wheel used in ceramic grinding, turning at 3500 rpm. Typical abrasive particles range from about 20 to 200 μm across (Hebbar, et al. 1992). For these parameters, a 20 μm particle tip passes a given point on the workpiece in about 30 μs. To measure the effects of such a process, the hot junction of a thermocouple would need to be on the order of 20 μm and have a response time of greater than 30 μs. Furthermore, the extremely low thermal conductivities of ceramics require any contacting temperature measurement device to be placed so close to the grinding that it will likely be destroyed before an accurate temperature indication can be given. These difficulties make non-contact, fast time-response methods such as optical temperature measurement much more accurate for flash grinding temperature measurement.

Other researchers have recognized the value of using infrared emission to determine grinding temperatures (see Section 1.2). The primary benefits are improved temporal and spatial resolution, the avoidance of conduction effects, and the possibility to determine the spatial distribution of temperature easily. Each of these benefits has been exploited in this study.

In this study, infrared imaging, which is a single-wavelength method, a dual-wavelength ratio method, and spectrometric methods provided qualitative spatial temperature distributions, very high speed temperature monitoring, and spectrum analysis temperature verification, respectively. The theory underlying each of these methods is discussed below.

4.2 Optical method theory

An understanding of the theoretical background of optical temperature measurement is valuable and will be presented here. Optical temperature measurement is possible because any object at a temperature above 0 K emits electromagnetic energy as photons, or bundles of light. The intensity and frequency (or wavelength) of the photon emission varies with the temperature of the source.

The correlation of intensity, wavelength (or frequency), and temperature is provided by Planck's distribution of blackbody radiation. It forms the basis of optical temperature measurement and is expressed in the following equation:

$$E_{\lambda,b}(\lambda,T) = \frac{C_1}{\lambda^5\left(e^{\frac{C_2}{\lambda T}} - 1\right)} \tag{4.1}$$

in which $E_{\lambda,b}$ is the blackbody emissive power ($W/m^2/\mu m$) at a given wavelength and temperature, T is the temperature (K) of the emitting surface, λ is the wavelength (μm) of concern, C_1 is a radiation constant equal to 3.742E8 $W \cdot \mu m^4/m^2$, and C_2 is a radiation constant equal to 1.439E4 $\mu m \cdot K$. The emissive power of a non-blackbody is the blackbody emissive power scaled by the emissivity. A material for which the emissivity is constant, and less than one, within a band of wavelengths is considered to be a graybody in that band. For radiation that passes through a material, the power at the receiving surface is the blackbody emissive power scaled by the emitting surface's emissivity and the transmitting surface's transmissivity. (Incropera and DeWitt, 1996) Planck's distribution and the definitions of emissivity and transmissivity form the basis of optical temperature measurement. Under certain conditions, these allow the intensities of optical signals to be interpreted as temperature indications.

A note should be made here on the terminology used in the discussion of thermal properties. For clarity, the suffix –ivity is used for the ideal material, which is optically smooth and homogeneous. The suffix –ance refers to values for an actual object. These values are related to surface phenomena, not solely to the bulk material properties. In consistency with these distinctions, -ivity will often be used in theoretical discussions, while –ance will be used in the discussion of experimental processes. (Touloukian, 1970)

4.2.1 Single-wavelength temperature measurement

The simplest of optical methods collects the signal at a single nominal wavelength or within a small band of wavelengths. The strength of this signal is typically converted to temperature, or calibrated, through one of two means, or variations of them. The first

requires that the correlation between the detector's output and the power of the incoming light, or the incident radiant power, be known. This information is often provided by the detector manufacturer. The incident radiant power may be related to the temperature of the source by Planck's blackbody law, given the emittance of the source and the transmittances of any materials in the path between the source and detector. Therefore, the emittances and transmittances of the participating materials must be determined in some way. This is most often done experimentally. It should be noted that a number of complications may and do arise from this method. In some cases, reflection of infrared signals from external sources may be involved. Additionally, the emittances and transmittances of materials often change with temperature and wavelength. Such complications may, and in fact must, be addressed to effectively use this method. The second calibration method is to heat the source through a range of known temperatures and record the detector output for each temperature. This eliminates the need to consider the source emittance explicitly. If possible, this is done in the same arrangement used for the experiments to eliminate the need to determine the transmittances of the intervening media as well.

These methods work well for some applications. However, in the case of grinding temperature measurement, a number of factors complicate such calibrations. Firstly, at any time, it is unclear which of the components are emitting. The infrared signal may be emitting from the grinding wheel abrasive, the binder, the workpiece, or a combination of any or all of these. Secondly, the workpiece and grinding abrasive in this case are known to transmit infrared radiation. Heat at the surface establishes temperature

gradients throughout the volume of each material. Since the emissive power varies with temperature, a gradient of emissive powers is established. For a transmitting material, the whole volume of emitting material within the view established by the detector optics is "seen" by the detector. This is very different from viewing a non-transmitting surface, in which only the surface participates. Since it is unknown, at any time, which components are emitting, and at what relative strengths, a theoretical approach to calibration is nearly impossible. Empirical methods fall short as well. A calibration based on heating each sample to a known temperature returns inaccurate results, since the materials of interest transmit radiation from within their volumes. An attempt to calibrate based on reproducing the temperature gradient requires that the very information sought in temperature measurement- the temperature at each given point. In light of these limitations, a method requiring no calibration would be beneficial.

4.2.2 Dual-wavelength temperature measurement

An alternative to the single-wavelength method addresses this need. The ratio method of infrared temperature determination solves a number of problems by making the simple assumption that the emittance and transmittance of any participating media, at a given temperature, vary little over any small band of wavelengths. Given that assumption, the temperature may be determined directly from the ratio of the detector strengths at two wavelengths in the band, without determining the emittance or transmittance of any participating media.

The assumption of spectrally constant (i.e., not varying with wavelength) emittance and transmittance can be verified by a number of methods. The first is through

consult ting previous research. Spectral emissivity and transmissivity curves are published for a number of materials (e.g. the Thermophysical Properties Research Center Data Series, edited by Touloukian), and these data were used for initial determinations of constant-value wavelength bands for each material. The second method is through direct measurement. The spectrometer used in the research is enabled for direct measurement of absorptance (α) and transmittance (τ). For an object at thermal equilibrium, conservation of energy dictates that the absorptance must be equal to the emittance at any wavelength, or $\alpha_\lambda=\varepsilon_\lambda$. This is Kirchoff's Law (Incropera and DeWitt, 1996), and it applies at all times, not just at thermal equilibrium. Therefore, by measuring the absorptance, the emittance is known as well.

The two-wavelength ratio method considers the power received, at each of two wavelengths, from a source of some temperature. By the blackbody equation, the received power at either wavelength can be used to determine the source temperature, if the emittance of the emitting surface and transmittances of any transmitting materials are known. If they are not known, but can be assumed to be constant between the two wavelengths, then the ratio of the received powers can be used to determine the source temperature. This is the basis of the ratio method, which is outlined below.

Begin with Planck's distribution, re-stated here:

$$E_{\lambda,b} = \frac{C_1}{\lambda^5\left(e^{\frac{C_2}{\lambda T}} - 1\right)} \tag{4.1}$$

The spectral emittance of an object is defined as the ratio of the actual emissive power at any wavelength to the blackbody emissive power at that wavelength, as shown here:

$$\varepsilon_\lambda = \frac{E_\lambda}{E_{\lambda,b}} \tag{4.2}$$

Combining the above two equation, the emissive power of a non-blackbody is defined as follows:

$$E_\lambda = \frac{\varepsilon_\lambda C_1}{\lambda^5 \left(e^{\frac{C_2}{\lambda T}} - 1 \right)} \tag{4.3}$$

The spectral irradiation G_λ received at a detector is further scaled by a factor known as transmittance, which is defined below:

$$\tau_\lambda = \frac{G_{\lambda,transmitted}}{G_{\lambda,incident}} \tag{4.4}$$

where $G_{\lambda,incident} = \varepsilon_\lambda E_{\lambda,b}$

Therefore the spectral radiation G_λ received at a detector, from a non-blackbody source of emittance ε, after passing through a material of transmissivity τ, is:

$$G_\lambda = \frac{\tau_\lambda \varepsilon_\lambda C_1}{\lambda^5 \left(e^{\frac{C_2}{\lambda T}} - 1 \right)} \tag{4.5}$$

The ratio R of the spectral radiation at each of two wavelengths may now be calculated as shown here:

$$R = \frac{\tau_{\lambda_1} E_{\lambda 1}(\lambda, T)}{\tau_{\lambda_2} E_{\lambda 2}(\lambda, T)} = \frac{\tau_{\lambda_1} \varepsilon_{\lambda_1} \lambda_2{}^5 \left(e^{\frac{C_2}{\lambda_2 T}} - 1 \right)}{\tau_{\lambda_2} \varepsilon_{\lambda_2} \lambda_1{}^5 \left(e^{\frac{C_2}{\lambda_1 T}} - 1 \right)} \tag{4.6}$$

If $\varepsilon_1 = \varepsilon_2$ and $\tau_1 = \tau_2$, then ε and τ don't affect R, as shown below:

$$R = \frac{\lambda_2{}^5 \left(e^{\frac{C_2}{\lambda_2 T}} - 1 \right)}{\lambda_1{}^5 \left(e^{\frac{C_2}{\lambda_1 T}} - 1 \right)} \tag{4.7}$$

Now, given R, λ_1, and λ_2, *T* may be determined. (DeWitt and Nutter, 1988)

4.2.3 Spectrometric temperature measurement

Two-wavelength, and other multiple-wavelength, ratio methods can be used to determine temperature by ratioing the strength of one signal to another. This may also be thought of as normalizing by one of the signals. It is, in effect, a scaling method. That is, the signal at one wavelength is scaled relative to the signal at another. If the emitted spectrum is assumed to originate from a graybody surface at all wavelengths of concern, then since the spectral behavior of graybodies is well defined, the temperature may be determined.

For spectrometric temperature measurement, the signals at a large number of wavelengths provide a portion of the received electromagnetic (or optical) spectrum. Two methods of analyzing this data are used in this study. One is a visual data fitting procedure, and the other is done by an explicit temperature equation. The theory behind each method is presented below.

4.2.3.1 Visual data analysis

The two-wavelength method involves an assumption about the shape of the received spectrum between the measured wavelengths. The shape is taken to be the same as a graybody at the temperature that causes the theoretical and measured intensities to be equal at the measured wavelengths. One drawback of such a method is that it depends on only two wavelengths to determine the shape of the curve. A spectrometer can be used to fill in the data between the measured wavelengths, more clearly defining the shape of the curve. Like a two-wavelength method, the spectrometer ratios received optical signals. Yet, because it provides the signals at many more wavelengths (the spectrometer used in

this research monitors 2048 distinct wavelengths), it describes the shape of the received spectrum more accurately than does a two-color method. It therefore provides a more accurate indication of the temperature of the source.

It has been stated that the shape of the received spectrum, or the relative intensities of adjacent wavelengths, is directly related to the source temperature, even for a graybody. This may be observed in the figures below. Consider first the blackbody curves. It is clear that the curves shape is different for each temperature. Now recall that a graybody curve is the blackbody curve corresponding to a certain temperature and scaled by some emissivity factor. In the case of practical measurements, there is often another unknown scaling factor. As long as all scaling factors are the same at each wavelength in a spectrum, one arbitrary scaling factor can be used for each spectrum. In

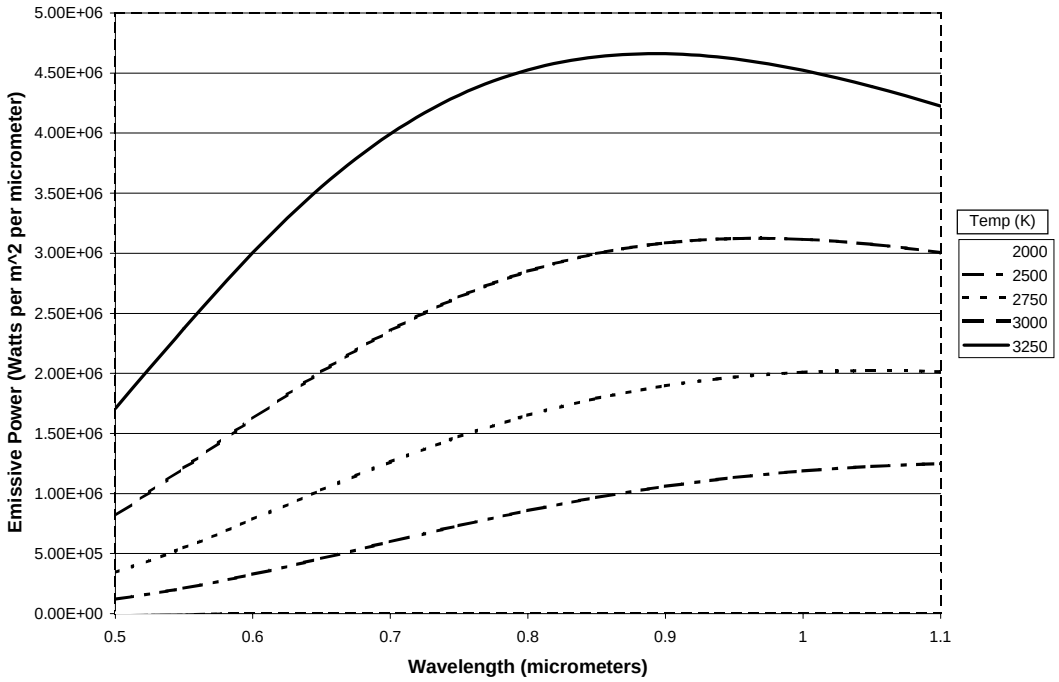

Figure 4.1: Blackbody curves

the figures below, each spectrum has been scaled by some factor such that all spectra intersect at some point. It is clear that they intersect at only one point. Then, in the wavelength ranges of concern, the curves of any two temperatures match at no more than one point. This allows a visual fit of the data to curves of known temperature.

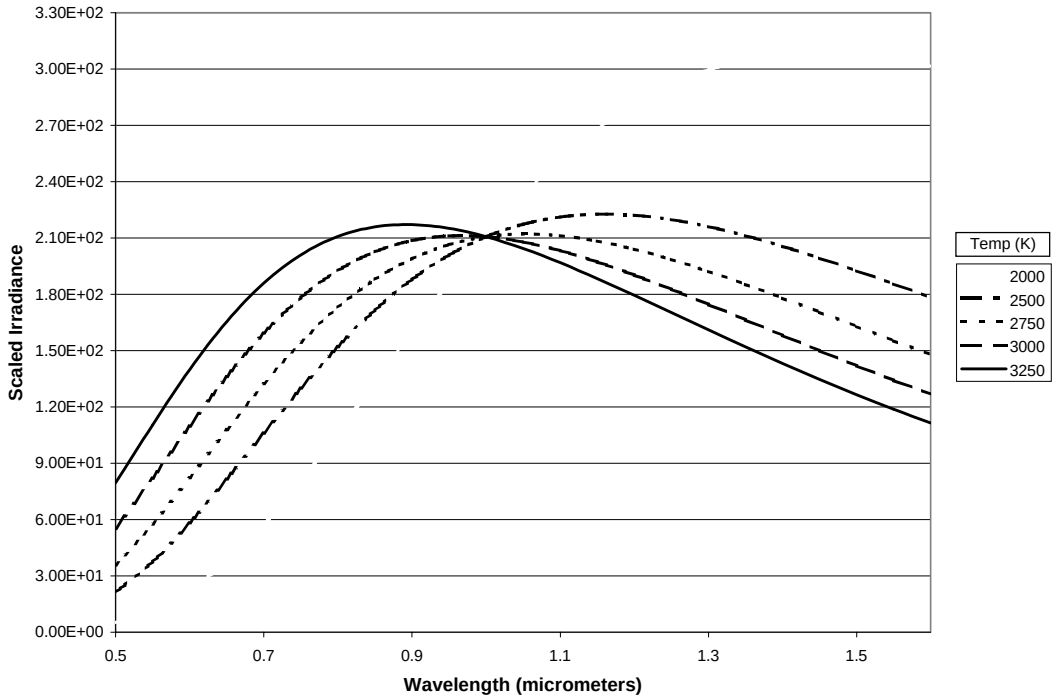

Figure 4.2: Blackbody curves scaling effect; intersection at 1.0 micrometers

For an indication of the experimental data's fit to thermal graybody behavior, each spectrum was visually fit to graybody curves of known temperature. Each graybody curve is a theoretical blackbody curve scaled by some value (which represents the emissivity, the transmissivity, and an arbitrary scaling factor between the spectrometer software's indication of relative irradiance and the irradiance incident on the spectrometer's array) such that the curves and the data all meet at one point. An example

is shown in Figure 4.3 below. The temperature curve that most closely follows the data at all other points is taken as a good approximation of the source temperature.

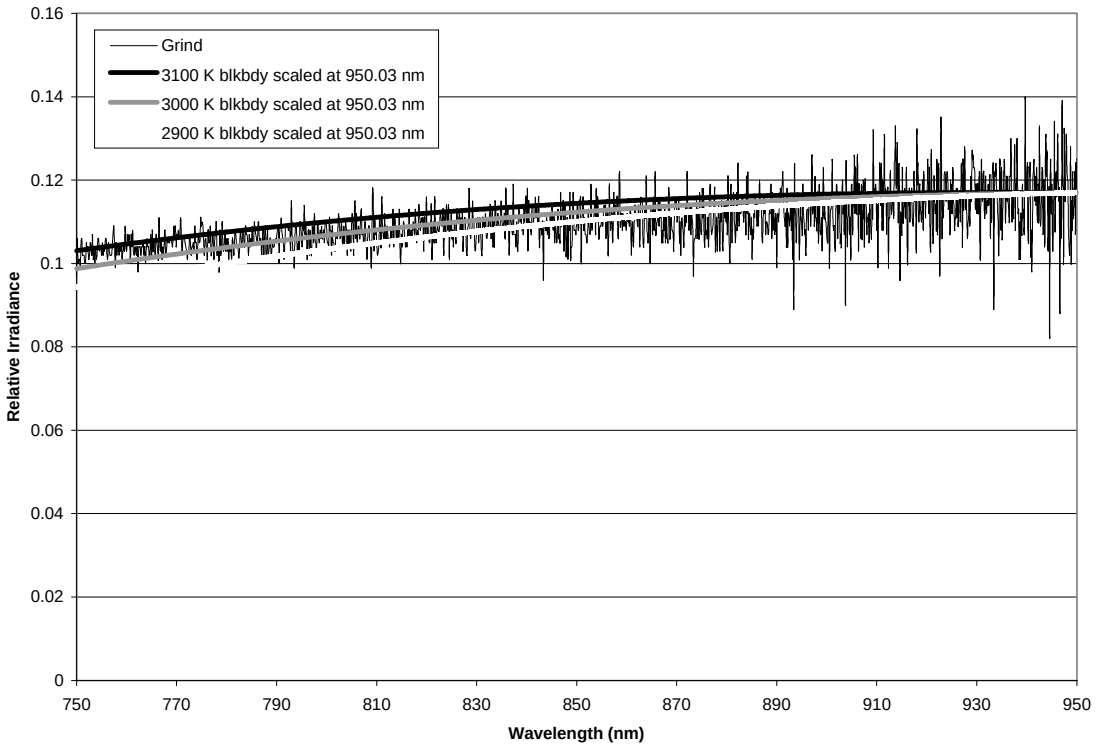

Figure 4.3: Sample of visual fit method, data from SiC grinding of MgO-PSZ

4.2.3.2 Explicit equation data analysis

The determination of an explicit equation for temperature (outlined below) has introduced a second method of temperature evaluation. In this method, experimental data provided by the spectrometer is entered into the explicit temperature equation at each wavelength. An unknown constant that applies to all wavelengths must be determined. For a theoretical case (a perfect graybody), the constant may be chosen such that the temperature is nearly equal at each wavelength. However, due to noise in the

experimental data, the temperature indication will always have some degree of variation related to noise. For experimental data, the constant was chosen such that a least squares line fit to the data has as near to zero slope as possible. This was accomplished through iteration on the scaling factor. To determine the uncertainty of this temperature indication, bounds were established for the slope of the best fit line. For one data set, the scaling factor was varied to obtain best fit line slopes of nearly $1x10^{-5}$ and $-1x10^{-5}$, and the difference in temperature indication was noted. This value was divided into the average between the two temperature indications to determine the bounds on the reported temperatures.

The derivation of the explicit temperature equation (Ng and Fralick 1999) begins with the equation, given previously, for the spectral radiation from a source of emissivity ε, after passing through a material of transmissivity τ:

$$G_\lambda = \frac{\varepsilon_\lambda \tau_\lambda C_1}{\lambda^5 \left(e^{\frac{C_2}{\lambda T}} - 1 \right)} \tag{4.5}$$

The equation is rewritten as follows, in order to simplify the derivation in a later step

$$G_\lambda = \frac{\varepsilon_\lambda \tau_\lambda C_1}{\lambda^5} e^{-\frac{C_2}{\lambda T}} \left(\frac{1}{1 - e^{-\frac{C_2}{\lambda T}}} \right) \tag{4.8}$$

The scaling factors ε and τ are now moved to the left side, giving:

$$\frac{G_\lambda}{\varepsilon_\lambda \tau_\lambda} = \frac{C_1}{\lambda^5} e^{-\frac{C_2}{\lambda T}} \left(\frac{1}{1 - e^{-\frac{C_2}{\lambda T}}} \right) \tag{4.9}$$

Taking the natural log of each side yields:

$$ln\left(\frac{G_\lambda}{\varepsilon_\lambda \tau_\lambda} \right) = \ln(C_1) - 5\ln(\lambda) - \frac{C_2}{\lambda T} + \ln(1) - \ln\left(1 - e^{-\frac{C_2}{\lambda T}} \right) \tag{4.10}$$

For the temperatures (~3000 K) and wavelengths (0.75 to 0.9 micrometers) of interest in this study, the remaining exponential term is approximately zero, so the above reduces to:

$$ln\left(\frac{G_\lambda}{\varepsilon_\lambda \tau_\lambda} \right) = \ln(C_1) - 5\ln(\lambda) - \frac{C_2}{\lambda T} \tag{4.11}$$

Rearranging yields:

$$\frac{1}{T} = \frac{\lambda}{C_2} \left[\ln(C_1) - 5\ln(\lambda) - ln\left(\frac{G_\lambda}{\varepsilon_\lambda \tau_\lambda} \right) \right] \tag{4.12}$$

And, finally:

$$T = \left\{ \frac{\lambda}{C_2} \left[\ln(C_1) - 5\ln(\lambda) - ln\left(\frac{G_\lambda}{\varepsilon_\lambda \tau_\lambda} \right) \right] \right\}^{-1} \tag{4.13}$$

Note that the explicit temperature equation above is wavelength-dependent. This is true because no assumption has yet been made about the relationship between temperature, wavelength, and spectral irradiance. It should be clear that the temperature of an object does not vary with the wavelength of the emitted spectrum. The irradiance, which varies with wavelength, results from an object at one temperature at any time. However, due to noise inherent in data collection, experimental data may indicate temperatures that vary with wavelength. The key to determining temperature with the above equation is then to find values for the emissivity and transmissivity that give the least variation in temperature across the band of wavelengths under consideration. The selection of values for emissivity and transmissivity will be discussed in greater detail below.

Before considering the selection of values for emissivity and transmissivity, another factor must be introduced. The spectrometer used in this study returns results not in $W/m^2/\mu m$, which are the units for spectral irradiance, but in terms of relative irradiance, which are unitless. Some unknown conversion factor S exists which relates the spectral irradiance to the relative irradiance. That is,

$$I_\lambda = SG_\lambda = S\varepsilon_\lambda \tau_\lambda E_{\lambda,b} \tag{4.14}$$

There are now three unknown factors. However, the explicit temperature equation may be written as:

$$T = \left\{ \frac{\lambda}{C_2} \left[\ln(C_1) - 5\ln(\lambda) - ln(C_3 G_\lambda) \right] \right\}^{-1} \tag{4.15}$$

where $C_3=(S\varepsilon_\lambda\tau_\lambda)^{-1}$ is a newly-defined constant which includes the conversion factor, emittance , and transmittance. The conversion factor S is a constant when the spectrometer is properly calibrated. Emittance and transmittance must be assumed constant with respect to wavelength to define the constant C_3. Determining the temperature is simply a matter of finding the value of C_3 that provides a best fit line with no slope.

For some theoretical analyses, the constant C_3 may be most easily determined for a given wavelength band by dictating that the temperature at any two wavelengths be equal. This stipulation results from the fact that, ideally, each wavelength should indicate the same temperature, as discussed above. The derivation of the equation for C_3 is outlined below.

Begin with the explicit temperature equation, given previously but restated below:

$$T=\left\{\frac{\lambda}{C_2}\left[\ln(C_1)-5\ln(\lambda)-ln(C_3G_\lambda)\right]\right\}^{-1} \tag{4.13}$$

The temperatures at any two wavelengths in the range of concern are set equal, yielding:

$$\frac{\lambda_1}{C_2}\left[\ln(C_1)-5\ln(\lambda_1)-ln(C_3G_{\lambda_1})\right]=\frac{\lambda_2}{C_2}\left[\ln(C_1)-5\ln(\lambda_2)-ln(C_3G_{\lambda_2})\right] \tag{4.16}$$

The constant C_2 may be cancelled from each side, and the terms containing C_3 grouped to yield:

$$\lambda_2\ln(C_3G_{\lambda_2})-\lambda_1 ln(C_3G_{\lambda_1})=\lambda_2\left[\ln(C_1)-5\ln(\lambda_2)\right]-\lambda_1\left[\ln(C_1)-5\ln(\lambda_1)\right] \tag{4.17}$$

The wavelength terms on the left side are now distributed and the natural log terms expanded, giving:

$$\lambda_2 \ln(C_3) + \lambda_2 \ln(G_{\lambda_2}) - \lambda_1 \ln(C_3) - \lambda_1 \ln(G_{\lambda_1}) = \lambda_2 [\ln(C_1) - 5\ln(\lambda_2)] - \lambda_1 [\ln(C_1) - 5\ln(\lambda_1)] \tag{4.18}$$

Grouping and isolating the C_3 terms gives:

$$(\lambda_2 - \lambda_1)\ln(C_3) = \lambda_2 [\ln(C_1) - 5\ln(\lambda_2)] - \lambda_1 [\ln(C_1) - 5\ln(\lambda_1)] - \lambda_2 \ln(G_{\lambda_2}) + \lambda_1 \ln(G_{\lambda_1}) \tag{4.19}$$

Finally,

$$C_3 = \exp\left(\frac{\lambda_2 [\ln(C_1) - 5\ln(\lambda_2)] - \lambda_1 [\ln(C_1) - 5\ln(\lambda_1)] - \lambda_2 \ln(G_{\lambda_2}) + \lambda_1 \ln(G_{\lambda_1})}{\lambda_2 - \lambda_1} \right) \tag{4.20}$$

These explicit equations for temperature T and the constant C_3 makes possible a number of theoretical and empirical analyses. These analyses will be presented as needed, in the "Results" section.

The visual and explicit equation methods of temperature determination have been presented. Each has benefits that are important for accurately characterizing acquired spectra. The explicit method provides a consistent, reliable method of arriving at a best-fit temperature. However, the only indication it provides is a single number for temperature. The visual method provides a quick means of verifying that each acquired spectrum matches the appropriate temperature curves throughout the spectrum.

4.2.3.3 Luminescence

Visual analysis provides another important contribution to spectrometric methods. The spectrum can provide indications of the misleading non-thermal optical phenomenon of luminescence. Luminescence is the emission of photons at distinct wavelengths (as opposed to thermal photonic emission, which occurs over a broad range of wavelengths), when electrons previously excited to a high atomic orbital fall to their normal lower orbitals. This happens in certain materials under certain conditions. The condition that causes the luminescence determines the type. For instance, luminescence caused by light is called photoluminescence, when it is caused by a chemical reaction it is called chemo-luminescence, and tribo- or mechano-luminescence is caused by breaking a material. It is the last example that is of concern in grinding ceramics. For the purpose of this paper, the phenomenon will be referred to as tribo-luminescence or simply luminescence.

Because of the nature of luminescence, it generally occurs over narrow wavelength bands. The wavelengths depend on the emitting material's atomic structure. However, in complex materials, research has shown that the spectra of luminescence may be broadened, as the effects of the various components overlap. It is therefore a hypothetical possibility that the luminescent spectrum from a material would resemble thermal behavior's broad wavelength nature. This possibility will be addressed in the "Discussion" section.

While the spectrum is expected to provide indications of luminescence, the two-wavelength method provides very little information about the spectrum. In fact, it provides only two points on the spectrum. Luminescence is therefore a potentially

significant problem in two-wavelength temperature measurement. If the material being measured luminesces at one of the measured wavelengths, the ratio and the corresponding temperature indication may be affected. A spectrometer maybe used to address this issue. Because luminescence from each element occurs at distinct wavelengths, it appears on a measured spectrum as sharp peaks. Thermally caused spectra, however, show much more gradual variations in the signal with wavelength. Therefore, the spectrometer should reveal if luminescence occurs at one of the wavelengths chosen for the two-wavelength method. This provides a check on one potential shortcoming of that method. The spectrometer may also be used to determine the temperature directly, after the spectral characteristics caused by luminescence (i.e., sharp peaks) have been visually distinguished from those caused thermally.

4.3 Optical measurement experiments

To date, three types of method of temperature evaluation have been used. They are: infrared imaging camera, two-wavelength ratio method (a category which includes two design iterations, each of which were implemented), and multi-wavelength ratio method (spectrometry). A description of each technique, along with its benefits and drawbacks, is presented below.

4.3.1 Imaging camera method

A Raytheon Radiance HS infrared camera, receiving light in the 3 to 5 micrometer wavelength band, was used to image the heat distribution across the workpiece during grinding. The camera was positioned outside of the grinding machine

and focused on a mirror within the fixture holding the workpiece. The distribution of heat generated at the workpiece surface during grinding causes the wheel and workpiece

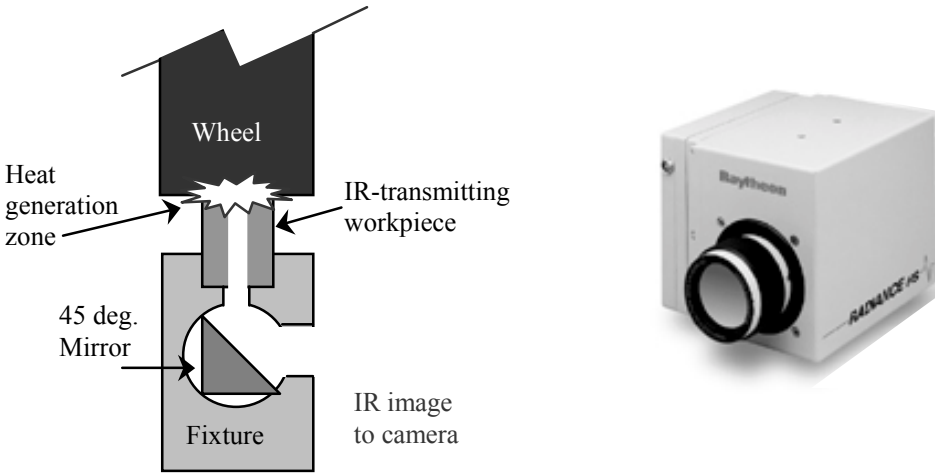

Figure 4.4 : Illustration of IR imaging fixture and picture of IR imaging camera

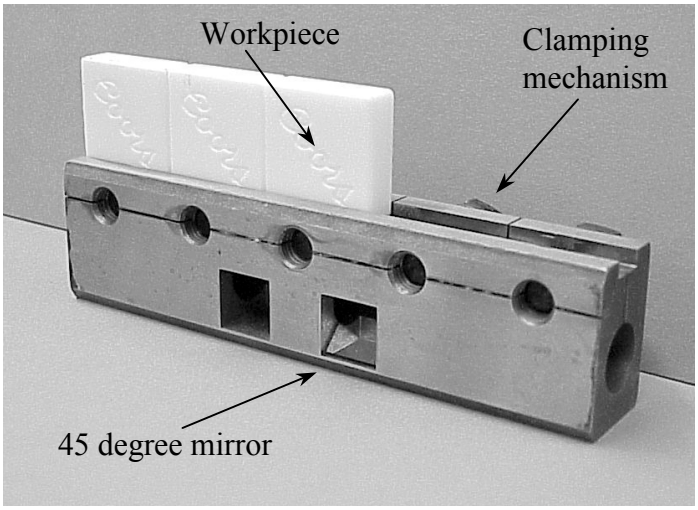

Figure 4.5: Tiles in grinding fixture for infrared camera

to emit a corresponding distribution of infrared light intensities. Once detected by an infrared camera and converted (in this case, by software) to an image in the visible range, this distribution may be called an infrared image. For simplicity, infrared image as used here will also refer to the infrared light emitted from the wheel and workpiece. Since our workpiece, MgO-PSZ, is semi-transparent in the infrared range, this image passes through the workpiece. The fixture and mirror were designed such that the infrared image that passes through the bottom of the workpiece is reflected by the mirror to the camera.

We achieved excellent qualitative results with this method. It provided maps of the temperature distribution across the workpiece. These temperature maps indicate that the region of highest temperature is at the center of the grinding zone.

However, the results are difficult to calibrate, and a reliable calibration was never achieved. Proper calibration requires knowledge of the spectral emissivity of the material being measured. This information is available for some materials in given states (Touloukian, et al., 1970). However, these values may not be valid for the grinding process, due to the differences in the conditions during grinding from the carefully controlled conditions used when measuring the published dada. One difference is that the wheel and workpiece are in contact during grinding and, therefore, both are heated and emit radiation. Another is that the emitting materials are in a high strain rate process during grinding. Finally, the emissivities of some materials are temperature-dependent.

The proposed method of calibration was to assume the grinding process emits as a blackbody (having an emissivity of one at all wavelengths). As discussed previously, for

a given temperature, a blackbody cannot emit a greater intensity of radiation at any wavelength. Calibrating was then simply a matter of correlating the camera's response to a blackbody of known temperature with the camera's response to the grinding process. The blackbody source used was a Mikron M305 blackbody oven. A plot of the correlation between blackbody oven temperature and camera output intensity was created for calibration. Determining the temperature was then simply a matter of finding the temperature that corresponds with the images captured during grinding.

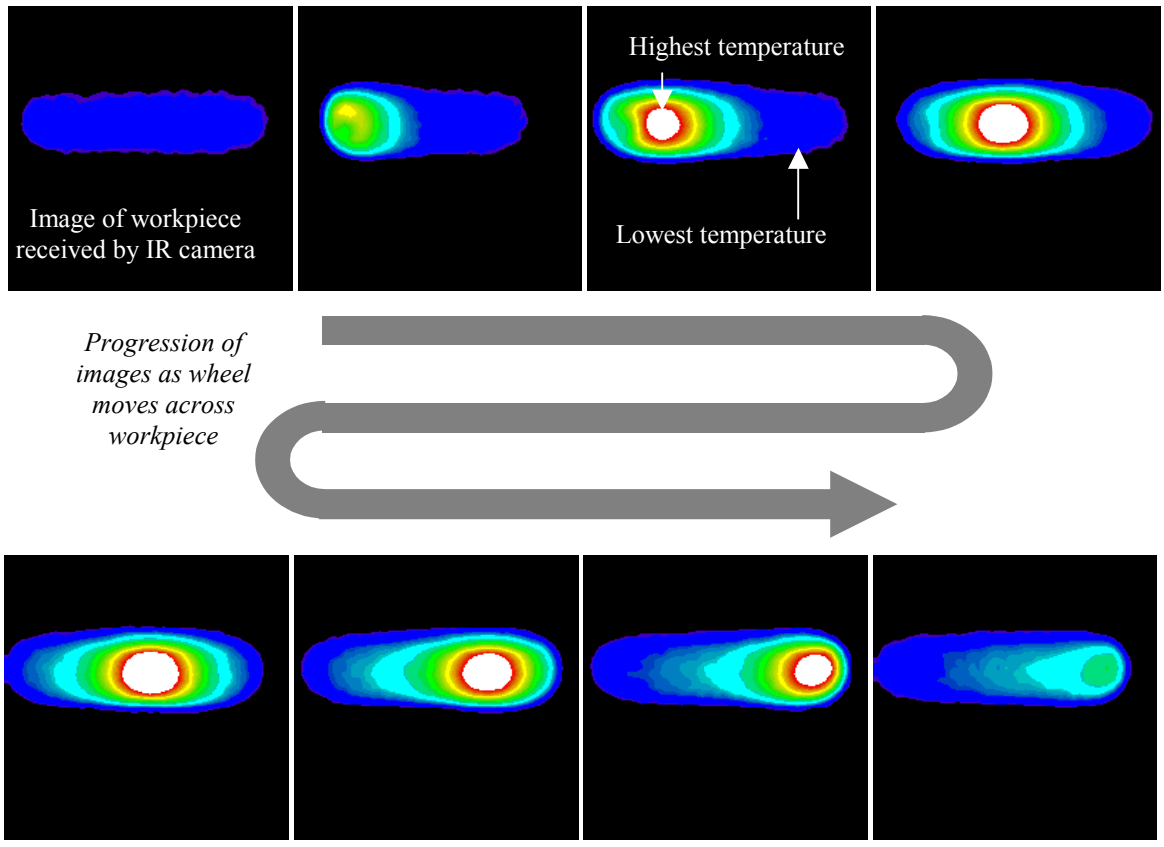

Figure 4.6: Results of infrared imaging camera test

4.3.2 Dual-wavelength method

To account for the fact that the emissivity of the process is not known, a two-wavelength ratio method was attempted. A significant advantage of this method is that the chosen detectors operate at very high speeds (over 1 MHz), so the grinding process may be analyzed with excellent time resolution. In fact, proof-of-concept tests reveal time variations in the heat generation that went undetected by other methods. Two variations of this method were devised, constructed, and tested. However, attempts at calibrating the methods were unsuccessful, so the desired temperature indications were not obtained. Each of the variations and the results from a proof-of-concept test will be presented here.

The dual-wavelength method, which eliminates the need to know the emissivity of the measured surface, is based on the assumption that two wavelengths can be chosen at which the emissivity is equal. Ensuring this typically requires that the wavelengths being used are nearly equal.

As mentioned, the two-wavelength ratio method underwent two iterations. The difference is primarily in how each directs the incoming signal to the two photodetectors. Neither has demonstrated acceptable repeatability. The first method uses a coarse grating

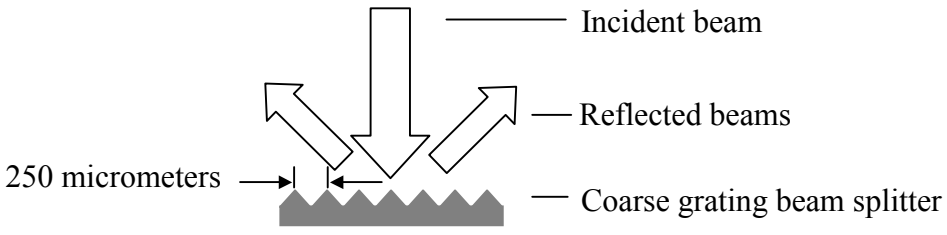

Figure 4.7:Oriel Instruments' coarse grating beam splitter

beam splitter supplied by Oriel Instruments. It is essentially an array of finely-etched mirrors angled to direct a collimated incoming beam evenly between two paths. Each path is opposite the other and 45 degrees from the incident beam. Although this method

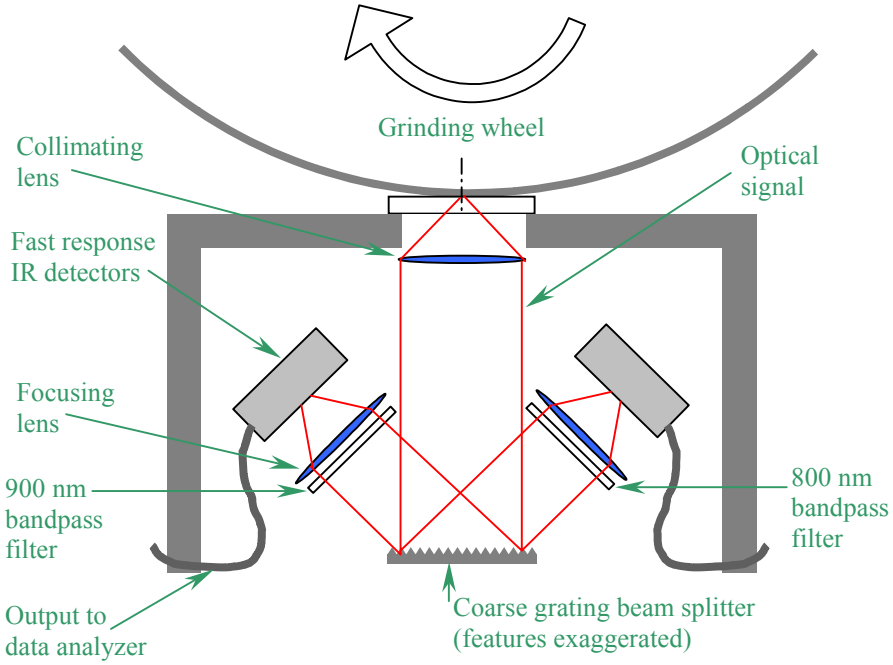

Figure 4.8: Schematic of dual-wavelength method with beam splitter

did provide adequately strong signals during grinding, a reliable calibration was not achievable. In attempting to calibrate the instrument, it was discovered that it produced inconsistent temperature indications when supplied with radiation from an optical fiber connected to a constant-temperature blackbody source. The indicated temperature depended on the position of the instrument relative to the fiber. Since the temperature indication for a two-wavelength method depends on the ratio of the signal at each detector, it is clear that the ratio of the incoming radiation varied with the source position.

This is thought to have resulted from internal reflections within the housing that contains the sensors and beam splitter.

To correct this error, a bifurcated optical fiber bundle was used in place of the beam splitter. The bundle consists of 950 fibers at the common end. Each fiber is of 50 micrometer diameter. The fibers are directed to either of two ends, each of which

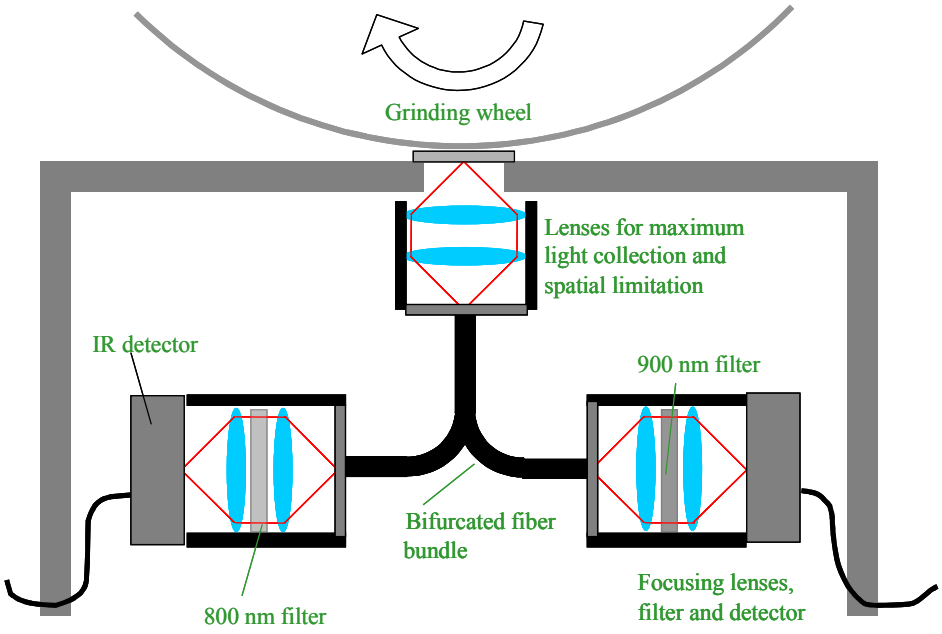

Figure 4.9: Schematic of dual-wavelength method with bifurcated fiber

connects to the appropriate filtered detector. The fibers are randomly divided between the two detectors, in the expectation that light falling on any part of the common end is evenly divided between the two detectors. However, if the fibers aren't perfectly randomized, the method fails to provide consistent ratios. Instead, the ratio varies depending on where the incident light falls, as illustrated in Figure 4.10 below. Calibration tests reveal that the ratio of the signals at each detector does, in fact, vary

with position. This indicates that the fibers are not statistically randomly directed. A valid calibration must be achieved before this method can be used for temperature measurement. Since that has not yet been achieved, further development of the ratio method is needed.

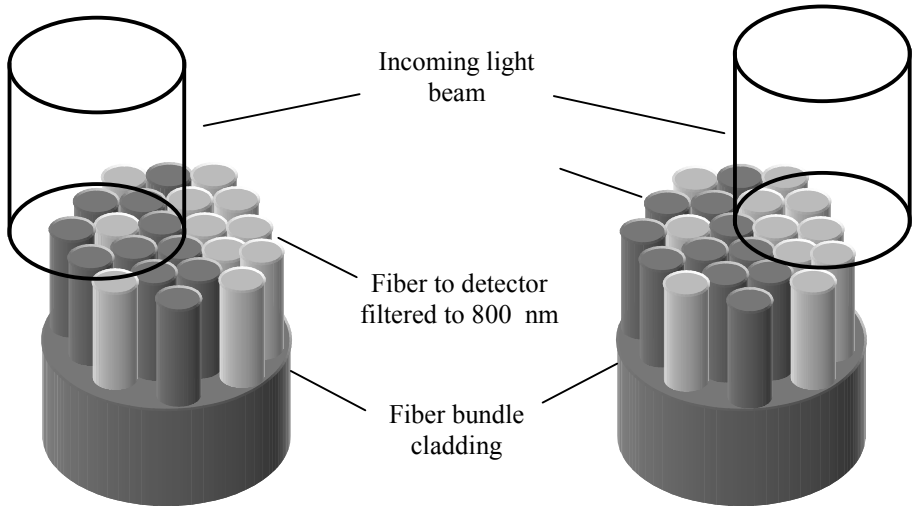

Figure 4.10: Illustration of error source in poorly randomized bifurcated fiber

In spite of the need for further development, valuable results were obtained from the two-wavelength ratio method using the bifurcated fiber and beam splitter. The advantage of this method is its excellent time response, and the information it reveals lies in the time-dependence of heat generation. Initial tests indicate rapid fluctuation in thermal emission from the grinding process. In fact, in tests on the Harig grinder, a periodic fluctuation is observed. Because tests have eliminated every known possible source of noise as the cause, it seems most likely to be related to the system's natural frequency. That is, the wheel is most likely vibrating in a direction normal to the workpiece surface. The ability to reveal such phenomena are a strength of this method.

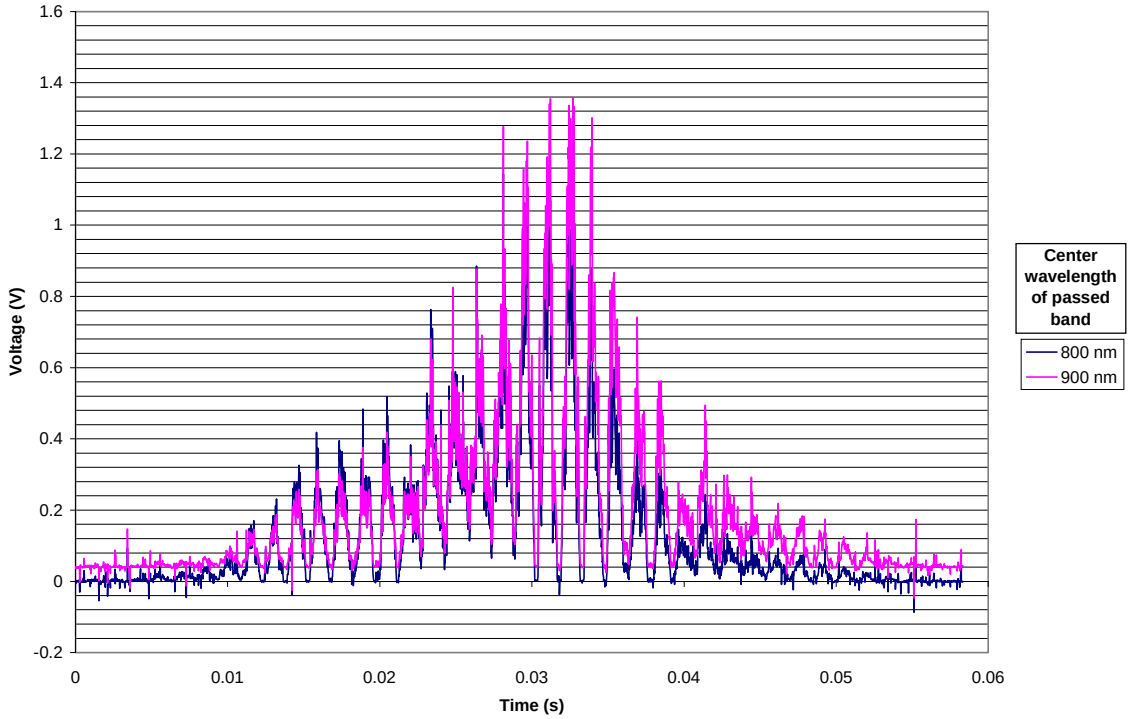

Figure 4.11: Results from dual-wavelength test, SiC grinding of MgO-PSZ

4.3.3 Spectrometric method

4.3.3.1 Spectrometer type

For this research, an Ocean Optics USB2000 spectrometer was chosen. It is a small, portable spectrometer that can be attached to a personal computer through its USB (universal serial bus) port. The wavelength band chosen was from 720 to 980 nm, or 80 nm above and below the wavelengths previously chosen for the two-wavelength ratio

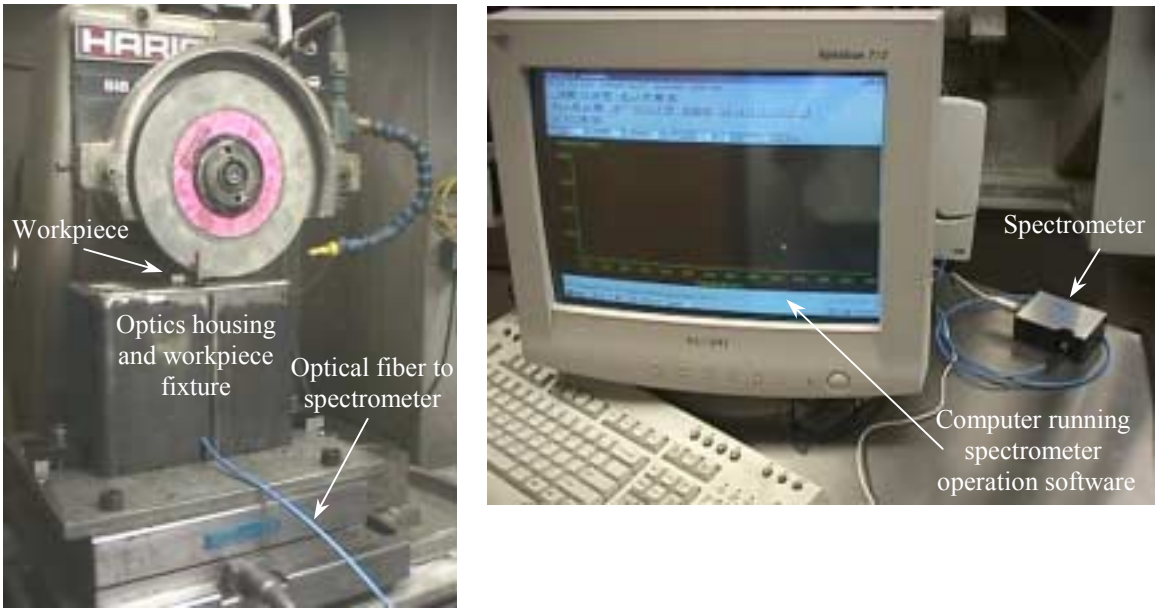

Figure 4.12: Spectrometric method arrangement

method. However, only the data from 750 to 950 nm was used, as the data at the beginning and end of each spectrum was significantly noisy. As mentioned previously, this spectrometer provides signals at 2048 wavelengths within the chosen band (720 to

980 nm). The resolution of the received signal is therefore great enough to reveal details a two-color method does not.

4.3.3.2 Spectrometer theory

The Ocean Optics USB2000 takes advantage of CCD (charge coupled discharge) arrays to create an innovative spectrometer. All spectrometers divide incoming light into its component wavelengths. Ocean Optics' spectrometers accomplish this with a diffractive grating. In order to convert each wavelength into a corresponding electrical signal, traditional spectrometers move a single detector through the field of wavelengths. This makes traditional spectrometers slow and susceptible to errors resulting from time variations in the spectrum. By using a CCD array, the USB2000 collects an entire spectrum at once. Each pixel on the array is in a position to receive a particular wavelength of light from the diffractive grating.

Optical signals from the source are carried to the USB2000 through an optical fiber. In the case of this research, a 600 μm diameter multi-mode fiber from Ocean Optics was used. The use of a fiber has two advantages. One is that the spectrometer can be located far from the source. Another is that the component wavelengths remain bundled until they enter the spectrometer, which is designed to control the distribution of the component wavelengths. Previous methods in this research have suffered from lack of control of the optical signal.

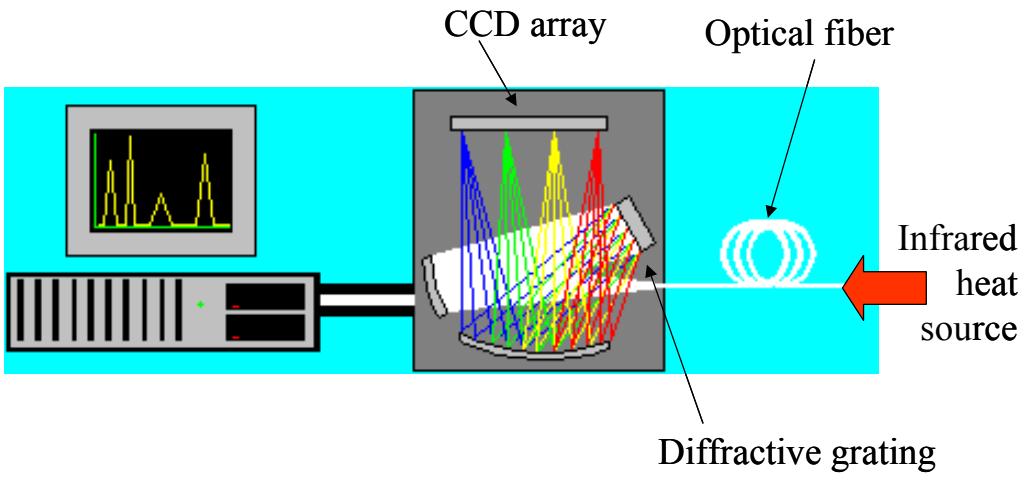

Figure 4.13: Schematic of spectrometric operation

4.3.3.2 Calibration method

The Ocean Optics USB2000 spectrometer must be calibrated to a known temperature blackbody source in order to obtain accurate spectra. The primary blackbody source used was a tungsten halogen incandescent lamp operating at 3100 K. Blackbody ovens at 1273 K and 2773 K were also used, both for calibration and for verification.

Calibration is the means by which each pixel in the spectrometer's CCD array is given the appropriate gain relative to the other pixels. This ensures that the relative intensities of each wavelength are correct, so the spectra are accurate. The process is as follows. First, the spectrometer input is blocked to provide a "dark signal", which is recorded to provide a baseline. Second, the temperature of a blackbody is entered into the operating software for the "reference signal". The spectrometer is then provided with the input from this blackbody of known temperature. This "reference signal" is recorded by the software as well. The software may then be used in "irradiance" mode. In this mode,

the software scales each wavelength appropriately to provide accurate spectra. For instance, in this mode, the signal from the blackbody source matches the shape of a theoretical blackbody (as described by the Planck distribution) at the same temperature.

It is important to recall that the relative intensities of each wavelength (which determine the shape of the curve), rather than the absolute intensities, for the spectrometer match that of the theoretical blackbody. It is neither possible nor necessary to compare intensities. It is not possible because the software provides only relative irradiance, which is unitless. The Planck distribution, on the other hand, provides true emissive power, in $W/m^2/\mu m$. It is also not necessary to compare intensities. The shape of a blackbody curve directly corresponds to its temperature. Therefore, for analysis purposes, the theoretical blackbody equation is scaled by some factor to make the values correspond with the output from the spectrometer.

Variations on the method of calibration were used during the study, with no significant difference in the results. The first method was to use a Mikron M305 blackbody oven at 1273 K. When the spectra recorded during grinding were found to indicate temperatures as high as 2773 K, a blackbody source of higher temperature was sought. A high-temperature blackbody oven in the Metrology Development Lab at Oak Ridge National Lab was used to calibrate the spectrometer at 2773 K, and the calibration was then verified with the Mikron oven at 1273 K. For later tests, a tungsten-halogen lamp corresponding to a 3100 K blackbody was used. In the case of the Mikron oven, adjusting the integration time of the spectrometer was adequate to provide the proper signal. However, when using the 2773 K oven, a neutral density filter was used to

prevent saturation of the spectrometer's CCD array. Initial calibrations with the lamp were performed through nominally neutral density filters and a special filter holder that required an additional optical fiber not used during grinding test. However, later calibrations with the lamp were performed through the workpiece and the grinding apparatus as used during testing. Attenuation through the workpiece alleviated the need for a neutral density filter, and the signal strength was once again modulated by adjusting the spectrometer integration time.

4.3.3.3 Sensitivity analysis method

As explained previously, each signal varies from a true blackbody by the scaling of unknown emissivity and transmissivity values, which may vary with wavelength and temperature. As long as there is no variation with wavelength or temperature, the signals recorded during grinding will have the shape of a blackbody curve at the source temperature. To account for the possibility of variations in these values, a sensitivity analysis was performed. This involved scaling the grinding spectra by a linearly varying series of factors. Scaling factors were used to compensate for the possibility of both 20% and 40% increases across the spectrum (720 to 980 nm) in the product of emissivity and transmissivity. Such spectral variations in the product of emisssivity and transmissivity would indicate artificially high temperatures. However, the possibility of such an occurrence is easily compensated for, by dividing the data by the desired scaling factor. For example, consider a data point at which it is assumed that the product of emissivity and transmissivity is 10% higher than nominal. That means its value is 1.1 times what is should be for the assumption of constant emissivity and transmissivity. To scale this

datum to return the proper temperature indication, it is simply divided by 1.1. After scaling an entire spectrum as desired, the "corrected" temperature was determined. This provides a measure of the sensitivity of the nominal temperature indication to the assumption of constant emissivity and transmissivity.

4.3.3.4 Overview of spectrometric tests

Two batteries of tests were conducted. Two spectrometers were used. The first group of tests was measured with an Ocean Optics S2000 spectrometer operating in the visible range (specifically, from 191 to 853 nm). It was used to measure the spectra generated by the grinding of MgO-PSZ with SiC on a Harig CNC surface grinder. An Ocean Optics USB2000 operating in the near infrared range (specifically, from 717 to 980 nm) was used for the rest of thes tests. Tests with it included the grinding of MgO-PSZ and AD995 alumina with SiC and diamond abrasive grinding wheels, on the Harig CNC surface grinder.

4.3.3.5 Results of spectrometric tests

All spectral tests conducted reveal a spectrum that closely resembles a graybody curve of very high temperature, from about 2500 K to 3100 K, depending on the wheel and workpiece types. The broadband natures of the spectra do not suggest luminescence. The tests indicate no variation in temperature with depth of cut or wheel speed.

The grinding temperatures are as follows. For SiC abrasive wheels grinding MgO-PSZ, the indicated temperature is about 3000 K. For SiC abrasive wheels grinding AD995, the indicated temperature is 2500 K. For diamond abrasive wheels grinding

MgO-PSZ, the indicated temperature is about 3000 K. For diamond abrasive wheels grinding AD995, no signal was registered.

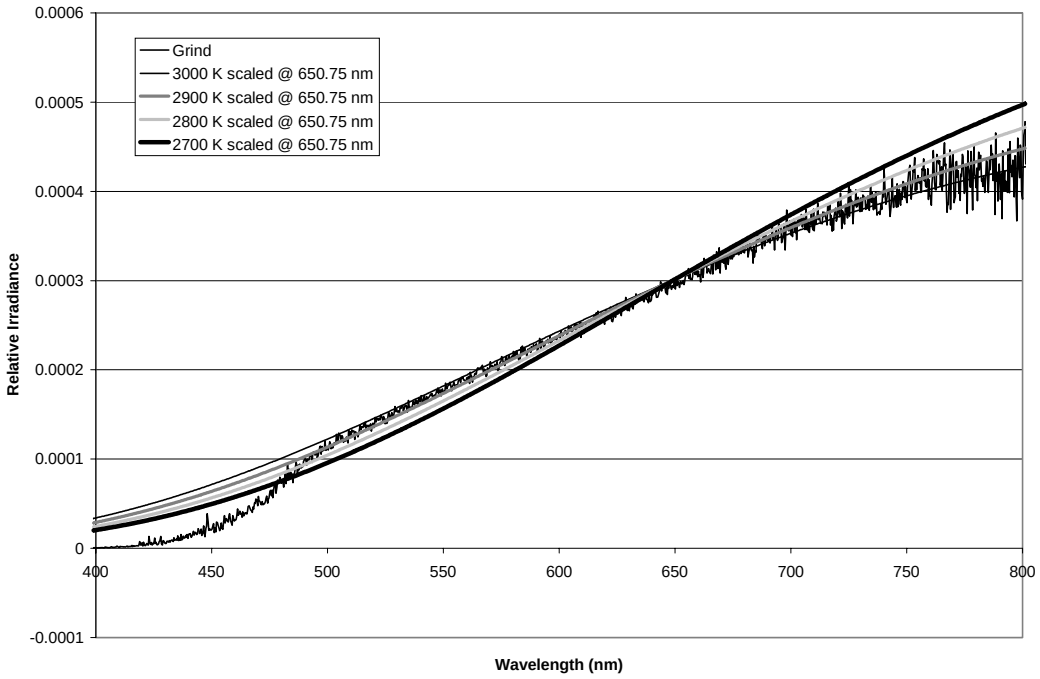

Figure 4.14: Representative visible spectrometer spectrum with visual curve fits For grinding of MgO-PSZ with silicon carbide

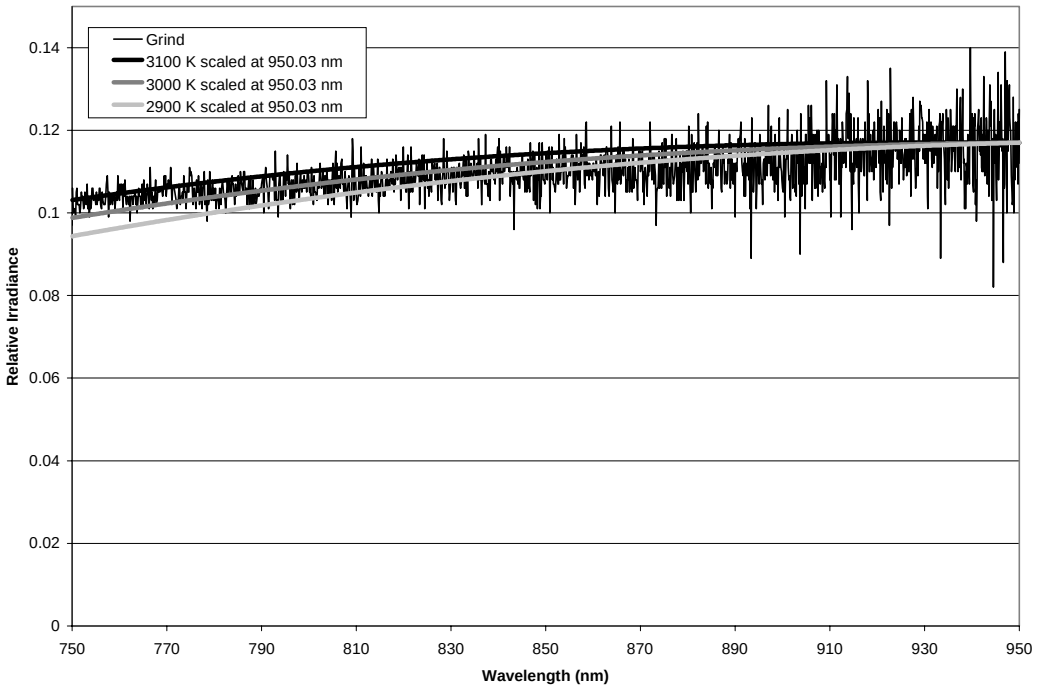

Figure 4.15: Representative near infrared spectrometer spectrum with visual curve fits For grinding of MgO-PSZ with silicon carbide

Table 4.1 Spectrometric test results, explicit temperature determination method

Group 2	SiC on TTZ			
Table speed	360	ipm		
Wheel speed	3500	rpm		
Downfeed	0.0001	in		
Thickness (in)	File	Grind	+/-10%	+/-20%
0.033	Test1_002a	3079	2667	2348
0.033	Test1_029	3082	2668	2349
0.015	Test7_011	3033	2633	2321
0.015	Test7_037	3050	2645	2331
	Average	**3061**	**2653.25**	**2337.25**
	Standard Dev'n	**23.59**	**17.17**	**13.62**

Group 3	SiC on TTZ			
Table speed	360	ipm		
Wheel speed	3500	rpm		
Downfeed	0.0002	in		
Thickness (in)	File	Grind	+/-10%	+/-20%
0.049	Test1_018	3051	2645	2330
0.045	Test2_005	3046	2641	2328
0.035	Test3_009	3022	2623	2316
0.020	Test5_006	2993	2601	2297
0.010	Test6_004	2586	2289	2050
0.010	Test6_030	2524	2239	2010
	Average	**2870.333**	**2506.333**	**2221.833**
	Standard Dev'n	**245.90**	**189.02**	**149.59**

Group 4	SiC on TTZ			
Table speed	360	ipm		
Wheel speed	3500	rpm		
Downfeed	0.0003	in		
Thickness (in)	File	Grind	+/-10%	+/-20%
0.048	Test1_015	2912	2541	2250
0.040	Test2_001	2957	2574	2276
0.030	Test3_024	2956	2573	2275
0.0055	Test5_007	2943	2563	2267
	Average	**2942**	**2562.75**	**2267**
	Standard Dev'n	**20.99**	**15.33**	**12.03**

Group 5	SiC on TTZ			
Table speed	360	ipm		
Wheel speed	4500	rpm		
Downfeed	0.0002	in		
Thickness (in)	File	Grind	+/-10%	+/-20%
0.05	Test1_008	2944	2565	2269
0.03	Test3_012	2995	2603	2299
0.025	Test5_010	3000	2607	2301
0.011	Test6_009	2982	2594	2291
0.011	Test6_034	2985	2596	2293
	Average	**2981.2**	**2593**	**2290.6**
	Standard Dev'n	**22.04**	**16.51**	**12.76**
	New Average	**2990.50**	**2600.00**	**2296.00**
	New Stdev	**8.43**	**6.06**	**4.76**

Group 6	SiC on TTZ			
Table speed	360	ipm		
Wheel speed	4000	rpm		
Downfeed	0.0002	in		
Thickness (in)	File	Grind	+/-10%	+/-20%
0.040	Test2_009	2989	2599	2295
0.040	Test2_035	3019	2621	2313
0.030	Test3_033	3003	2609	2303
0.020	Test4_039	3003	2610	2303
0.010	Test5_002	2986	2596	2293
	Average	**3000**	**2607**	**2301.4**
	Standard Dev'n	**13.19**	**9.92**	**7.92**

Summary1	SiC on TTZ	
	Average	**2965.043**
	Standard Dev'n	**44.15724**

Group 9	SiC on AD995			
Table speed	360	ipm		
Wheel speed	3500	rpm		
Downfeed	0.0001	in		
Thickness (in)	File	Grind	+/-10%	+/-20%
0.049	Test1_005	2424	2161	1947
0.049	Test1_049	2418	2156	1943
0.048	Test2_003	2363	2112	1907
0.048	Test2_029	2387	2131	1922
	Average	**2398**	**2140**	**1929.75**
	Standard Dev'n	**28.41**	**22.82**	**18.71**

Group 12	Diamond on AD995	
Table speed	360	ipm
Wheel speed	3500	rpm
Downfeed 1	0.0001	in
Downfeed 2	0.0002	in
Downfeed 3	0.0005	in
Note		
No noticeable signal at any downfeed		

Group 13	Dia. on TTZ			
Table speed	360	ipm		
Wheel speed	3500	rpm		
Downfeed	0.0001	in		
Thickness (in)	File	Grind	+/-10%	+/-20%
0.048	Test1_005	3255	2807	2462
0.046	Test2_031	3038	2643	2334
0.045	Test3_035	3204	2788	2460
0.040	Test4_000	3156	2739	2414
0.040	Test4_027	2897	2535	2249
	Average	**3110**	**2702.4**	**2383.8**
	Standard Dev'n	**143.64**	**113.09**	**91.49**

Group 14	Dia. on TTZ			
Table speed	360	ipm		
Wheel speed	3500	rpm		
Downfeed	0.0002	in		
Thickness (in)	File	Grind	+/-10%	+/-20%
0.039	Test1_013	3031	2638	2330
0.033	Test2_005	2991	2601	2297
0.028	Test3_011	2916	2545	2254
0.028	Test3_038	2960	2581	2284
	Average	**2974.5**	**2591.25**	**2291.25**
	Standard Dev'n	**48.64**	**38.84**	**31.49**

Group 15	Dia. on TTZ			
Table speed	360	ipm		
Wheel speed	3500	rpm		
Downfeed	0.0003	in		
Thickness (in)	File	Grind	+/-10%	+/-20%
0.027	Test1_012	2934	2557	2263
0.022	Test2_039	2924	2550	2257
0.014	Test3_006	2911	2540	2249
0.013	Test4_009	2914	2542	2251
	Average	**2920.75**	**2547.25**	**2255**
	Standard Dev'n	**10.44**	**7.80**	**6.32**

Summary2	Diamond on TTZ	
	Average	**3010.077**
	Standard Dev'n	**121.4005**

4.4 Discussion

It will be shown that previous measurements of asperity contact temperatures report temperatures as high as those we measure. It will furthermore be shown that the optical method employed in this study does not indicate an average of the temperatures in the field of view, but the peak, or asperity, temperature.

4.4.1 Comparison with temperature measurements of other researchers

Perhaps the most notable results of this study are the unexpectedly high grinding interface temperatures indicated. A review of the present literature in grinding temperature measurement reveals that the temperatures indicated in this study exceed previous researchers' results significantly. As will be shown, some of these methods considered other wheels and workpieces. More significantly, most depended on spatial or temporal extrapolations to evaluate background interface temperatures or wheel surface temperatures, rather than flash temperatures at the interface. Furthermore, it will be shown that the results from this study may be reasonable values for such flash temperatures. Validation of this hypothesis will require further investigation, primarily consisting of modeling techniques.

Consider first the results from previous empirical studies. An overview of these results is presented in Tables 4.1, 4.2, and 4.3. These results are considered in the following categories, according to the location of temperature measurement: Workpiece subsurface, Wheel viewed through a hole, Wheel surface after leaving grinding zone, and Interface.

Table 4.2: "Blind hole subsurface" temperature measurement studies

Reference	Measurement Method	Calibration Method	Abrasive	Workpiece(s)	Temperature(s)	Conditions
Ueda et al. 1992	Single wavelength	Workpiece heated to known temperatures	Resin-bond diamond wheel	Silicon nitride, silicon carbide, aluminum oxide	~1100 K	Silicon nitride, extrapolation to surface
Zhu et al. 1995	Single wavelength	2-wavelength emissivity determination	Diamond wheel	Silicon nitride	~1100 K	~0.05 mm depth
Kohli et al 1995	Thermocouple welded into hole	Thermocouple calibr'n	Vitrified aluminum oxide B150L100VZ wheel 100CBN wheel	AISI 52100 AISI 52100 AISI 52100	~800 K ~400 K ~400 K	At surface At surface At surface

Table 4.3: "Thru-hole to wheel surface" temperature measurement studies

Reference	Measurement Method	Calibration Method	Abrasive	Workpiece(s)	Temperature(s)	Conditions
Hebbar et al. 1992	Triple wavelength	Ratio method; constant emissivity assumption	Diamond indenter	Zirconia	~1900 K	Average temp
			Diamond indenter	Zirconia	~2000 K	Peak temp
			Diamond wheel	Zirconia	~1600 K	Peak temp
Chandrasekar et al. 1990	Single wavelength	Emissivity determination by heating and comparing radiation to blackbody and by multi-wavelength methods	Diamond indenter	Ferrite	~900 K	Peak temp
			Diamond indenter	Steel	~1500 K	Peak temp
			Resin bond diamond wheel	Ferrite	~1300 K	Peak temp
Farris and Chandrasekar 1990	Single wavelength	Emissivity determination by heating and comparing radiation to blackbody	Diamond indenter	Ni-Zn ferrite	~950 K	Average temp for highest wheel velocity
				Sapphire	~1550 +/- 80 K	Average temp for highest wheel velocity

Table 4.4: "Interface" temperature measurement studies

Reference	Measurement Method	Calibration Method	Abrasive	Workpiece(s)	Temperature(s)	Conditions
Farris and Chandrasekar 1990	Single wavelength, transmission through workpiece	Emissivity determination by heating and comparing radiation to blackbody	Diamond indenter	Sapphire	~1500 K	Mean temp
Griffioen et al. 1986	Single wavelength, transmission through workpiece	Emissivity determination by heating and comparing radiation to blackbody	Silicon nitride indenter	Sapphire	~3000 K	Peak temp
Outwater and Shaw 1952	Toolwork thermocouple	Thermocouple calibration	SiC wheel	SAE 1008 mild steel	~1650 K	

Table 4.5: "Wheel surface after leaving grinding zone" temperature measurement study

Reference	Measurement Method	Calibration Method	Abrasive	Workpiece(s)	Temperature(s)	Conditions
Ueda et al. 1985	Single wavelength	Emissivity determination by heating and comparing radiation to blackbody	Vitrified aluminum oxide	55% carbon steel	~1700 K	Peak temp, 45 deg. (4.2 ms) after grinding zone

The first group, denoted “Blind hole subsurface” (Ueda et al. 1992; Zhu et al. 1995; and Kohli et al. 1995), consists of those methods that measure the temperature below the grinding surface. These were done by monitoring the temperature of the upper surface of a blind hole drilled into the workpiece from the bottom. These studies measured the temperature response as the distance from the measured surface (the upper surface of the blind hole) to the grinding surface decreased with subsequent passes of the wheel. These results are reported as a function of distance from the grinding surface. In some cases, a curve was fit to the data to extrapolate the temperature at the grinding surface. In other cases, the final data point is reported at the surface. For either surface temperature indication, it is important to note that, until the distance of the measurement from the grinding surface is very small (approximately on the order of the distance between individual grits), conduction effects dictate that the temperature of an individual grit cannot be resolved. Even if the thickness is small enough to resolve individual grits, high spatial resolution of the measuring equipment is necessary. These subsurface temperature indications were not obtained by a high-resolution method, so it is certain that the background, rather than a flash, temperature is being measured. For data points reported to be at the surface, one of two conditions may exist. The first is that the part still has some minimal thickness. That is, measurements are taken below the surface by some distance the investigators considered negligible. In this case, the background temperature is still being measured, as discussed above. The other possibility is that these measurements are truly measurements for zero thickness, in which case the wheel surface is actually being observed as it passes over a hole in the workpiece.

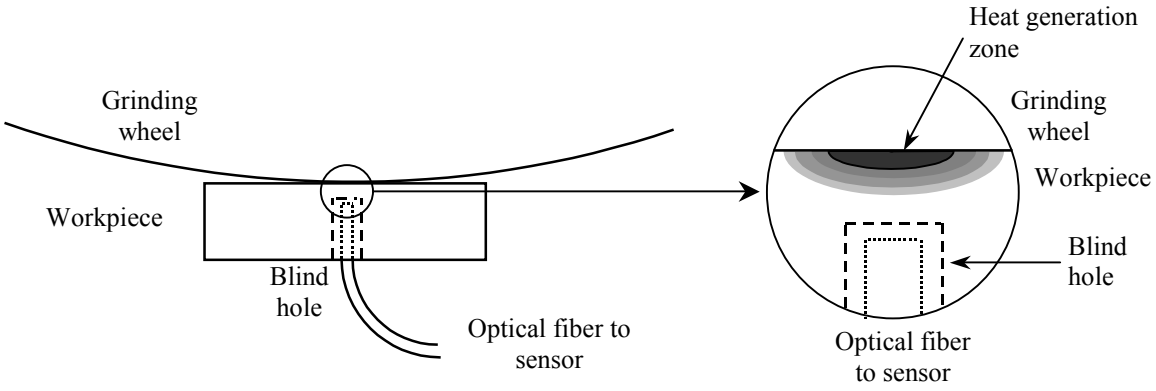

Figure 4.16: "Blind hole subsurface" test arrangement

The second and third types of published empirical method collect and analyze the optical radiation emitted by the wheel. The method denoted "Thru-hole to wheel surface" (Hebbar et al. 1992; Chandrasekar et al. 1990; Farris et al. 1990) observes the radiation passing through a hole in the workpiece, and "Wheel surface after leaving grinding zone" (Ueda, et al. 1985) provides temperatures at various points along the periphery of the wheel after engaging the workpiece. In each case, the temperature of the wheel is measured after leaving the grinding zone. This does provide an indication of the temperature rise of the wheel surface, but since it doesn't observe the grinding process, it provides no measure of the flash temperature.

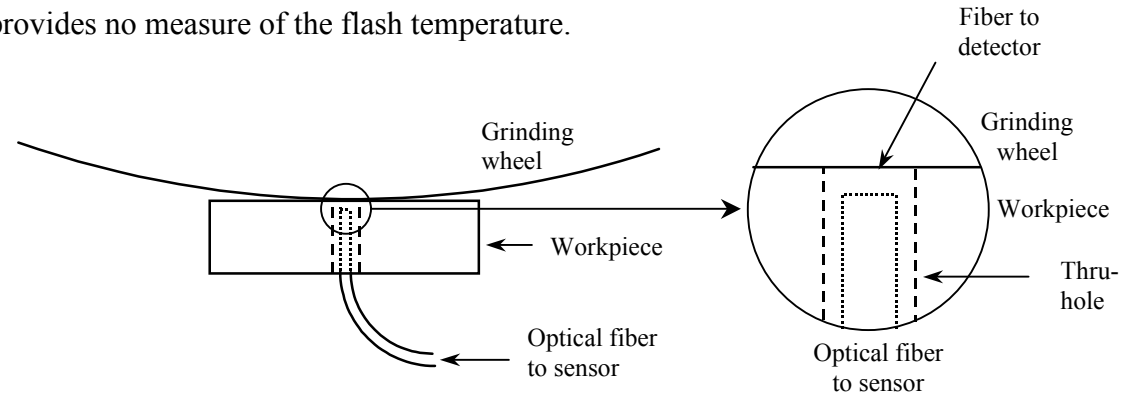

Figure 4.17: "Thru-hole to wheel surface" test arrangement

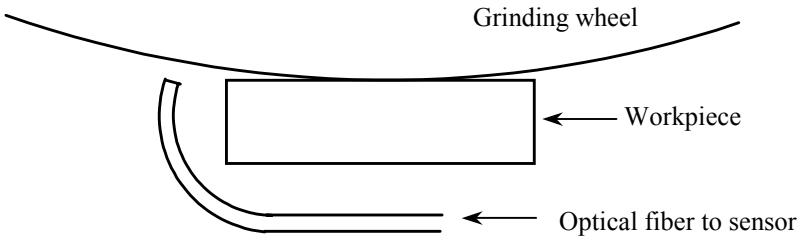

Figure 4.18: "Wheel surface after leaving grinding zone" test arrangement

Finally, results are reported of true interface temperature in grinding and in fundamental rubbing studies. The grinding interface method presented by Outwater and Shaw (1952) employs the toolwork thermocouple method, in which dissimilar metals are smeared across the grinding surface by the wheel. The smeared region provides a hot junction in a thermoelectric circuit. Such a method, which Outwater and Shaw (1952) applied only to metal workpieces, provides an average temperature indication over the hot junction, and not a flash temperature.

Farris and Chandrasekar (1990), and Griffioen, et al. (1985) present the methods most applicable to this study. In each of these studies, asperity contact temperatures are measured at the interface between a spinning sapphire disc and an indenter. As will be demonstrated, such asperity contact temperatures are most likely the temperatures being measured in the present study. In the study by Farris and Chandrasekar (1990), one method employs a through-hole to transmit the optical emission from the pin. In each study, the optical emission is also allowed to pass through the infrared-transmitting disc.

The temperature measured in these cases is therefore a true asperity temperature. Griffioen, et al. (1985) report temperatures as high as 3000 K by using this method.

4.4.2 Independence of temperature on wheel speed and downfeed rate

Another notable, and unexpected, indication of the current research is the independence of temperature from wheel speed and downfeed rate. As this was not the primary objective of the investigation, it has been examined for only one wheel/workpiece combination. However, the results of these tests are intriguing and deserve further investigation.

Temperature measurements were made for the grinding of MgO-PSZ with SiC. Downfeed rates and wheel speeds were varied independently. Downfeed rates were varied among 2.54 μm, 5.08 μm, and 7.62 μm, each at a wheel speed of 3500 rpm and table speed of 9 meters per minute. The first observation is that the intensity of the signal doubled for a doubling of the downfeed rate and tripled when the downfeed rate was tripled. The temperature indication, however, remained constant at 3000 K. For investigation of wheel speed effects, values of 3500, 4000, and 4500 rpm were used, while maintaining a downfeed rate of 5.08 μm and a table speed of 9 meters per minute. In each case, the temperature indication was 3000 K. These tests may indicate the dependence of temperature indication on the wheel/workpiece combination alone, at least within some range of values for downfeed, wheel speed, and table speed.

It may be suggested that these results indicate that luminescent, rather than thermal, radiation is being observed. This would explain the consistency of the spectra

for a given material. Such a suggestion is important because, as discussed previously, luminescent radiation does not indicate source temperature. However, the test results discussed below discount this theory of luminescence.

To investigate the possibility of luminescence, each material was ground with both diamond and SiC wheels. If the radiation were due to luminescence of the workpiece, the same spectra would result regardless of the abrasive type used to machine the workpiece. This is because mechanoluminescence results from atomic transitions in the source material, which behave consistently regardless of the exciting material. However, at least one test indicates temperatures that depend on the wheel/workpiece combination, not simply on the workpiece. Specifically, the grinding of AD995 with SiC generates spectra that match a graybody of 2500 K, while grinding it with diamond provides no detectable spectra. These tests further suggest that the detected spectra do, in fact, originate from a thermal source.

One might observe that the above holds true only if the workpiece luminescence doesn't vary with temperature. Perhaps the luminescence characteristics change appreciably with small changes in the workpiece temperature. According to such a theory, luminescent spectra would be generated by each material and, as the workpiece temperature varies slightly with different abrasive wheels, the emitted spectra could appear to indicate varying graybody curves. However, a luminescent source seems unlikely in light of the excellent match of the detected spectra with graybody curves for both alumina and MgO-PSZ.

The final positive indication for a thermal source is the consistency of spectra in the visible range with the near infrared range. Two spectrometers, one operating from 200 to 850 nm and the other from 720 to 980 nm, were used in tests of SiC and diamond abrasive wheels grinding MgO-PSZ. In each case, the spectra generated during grinding indicate temperatures of 3000 K for SiC grinding of MgO-PSZ and 3100 K for diamond grinding of MgO-PSZ. Note that some of the visible spectra deviate from the graybody curve below about 500 nm. This is most likely due to the decreased transmissivity or emissivity of MgO-PSZ from 200 to about 500 nm. However, as the visible spectrometer is no longer in the researchers' possession, this hypothesis has not been validated by measuring the transmissivity in this wavelength range.

4.4.3 Theoretical analyses

4.4.3.1 Spatial averaging

One matter of concern in using infrared radiation for temperature determination is the discrimination of multiple temperatures within the field of view. Researchers have noted that the presence of multiple temperature values within the field of view results in a temperature indication that is an average of the temperatures present (Griffioen, et al., 1985). That is, when looking at a hot spot which does not fill the field of view of the detector, the temperature indicated by the detector is lower than the actual hot spot temperature. While it is true that the presence of lower temperatures *tends* to lower the indicated temperature, the extent of its effect should be characterized. The results of such a characterization are reported below.

For the present analysis, the emission of wavelengths from 0.75 to 0.95 micrometers, within a field of view comprised of two temperatures, will be considered. The temperature indicated by the detector will be called the "effective temperature". It will be shown that a very large difference between the two temperatures yields a more accurate effective temperature. As the difference in temperatures decreases, the effect of the lower temperature becomes more pronounced. However, the effect produces a very low error even as the lower temperature approaches the higher temperature. This is because when the lower temperature approaches the higher, the average of the temperatures does not differ greatly from the higher temperature, so the error is still relatively low. As the temperature difference continues to decrease, the average moves progressively closer to the high temperature and the accuracy increases again.

This behavior is easily explained by considering the blackbody curves for different temperatures. Recall two characteristics of these curves. First, the shape of each curve, or the relative values of the power at adjacent wavelengths, is directly dependent on the temperature. Second, the blackbody curves give the emissive power, in $W/m^2/\mu m$, of blackbody sources at various temperatures and wavelengths. Since the power is given per unit area, the area of each temperature source must be considered. Consider a unit area field of view, with some fraction filled by a source of one temperature, and the rest comprised of a source of the other temperature. Now, in the 0.75 to 0.95 micrometer range, the emissive power of a low temperature (less than about 1000 K) source is less than for a high temperature (greater than about 3000 K) source by no more than 0.0041%. That means that in order for a blackbody source of 1000 K or less to affect the

temperature indication from a source of 3000 K, the area of the 1000 K source would have to be hundreds of times greater than that of the 3000 K source.

The exact behavior of the temperature averaging depends on the temperatures of concern and the emittances of each source. Effective temperatures for a variety of situations are reported here. For this analysis, effective temperatures of 3000 K are under consideration. Therefore, it is desired to determine the effective temperature when a field of view is comprised of a temperature of 3000 K and of a lower temperature.

The method for determining these effective temperatures was to add the emissive powers from two sources, one being at the higher temperature and the other being at a lower temperature. Using Equations 4.13 and 4.20, derived previously, an effective temperature was determined from this hypothetical data. The area of each temperature source is assumed to be equal. For a unit viewed area (i.e., $1m^2$), this amounts to a scaling factor of 0.5 m^2 for the emissive power from each source. However, since the scaling factor for each is equal, however, its effect may be included in the constant C_3, which is calculated as explained in Section 4.2.3 to determine the effective temperature.

The results, shown in Figures 4.17 and 4.18, clearly indicate excellent correlation of the effective or indicated temperature with the higher temperature. The poorest correlation occurs when the emissivity of the low temperature is high or the emissivity of the low temperature is low. In any case, the indicated temperature is always close to the highest temperature in the field of view. For this study, that suggests the temperature measurements are accurate indications of flash temperatures, rather than spatial averages of the temperatures within the spectrometer's field of view.

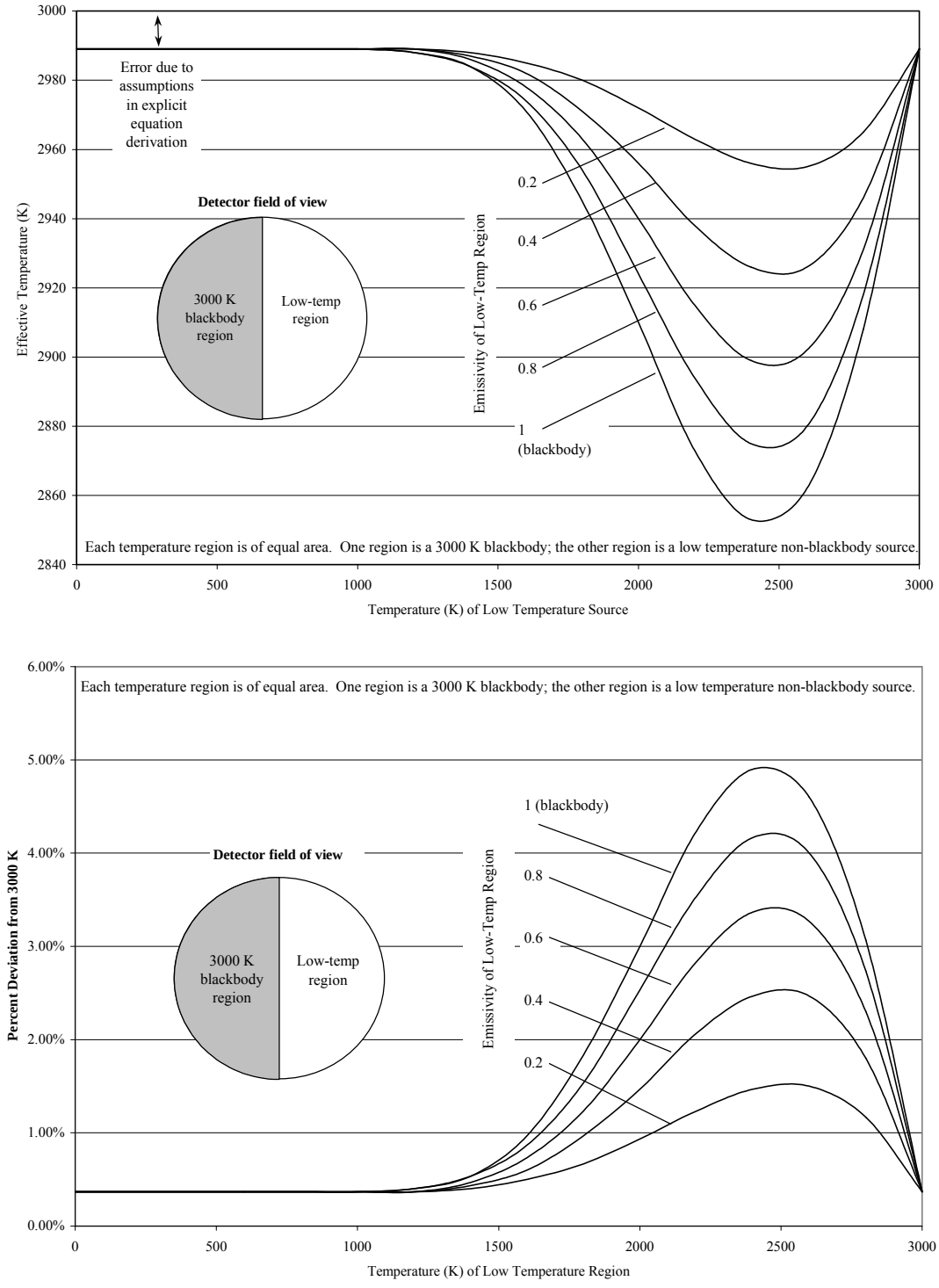

Figure 4.19: Effective spectrometric temperatures from dual-temperature source, 1 3000 K blackbody and lower temperature region of various emissivities

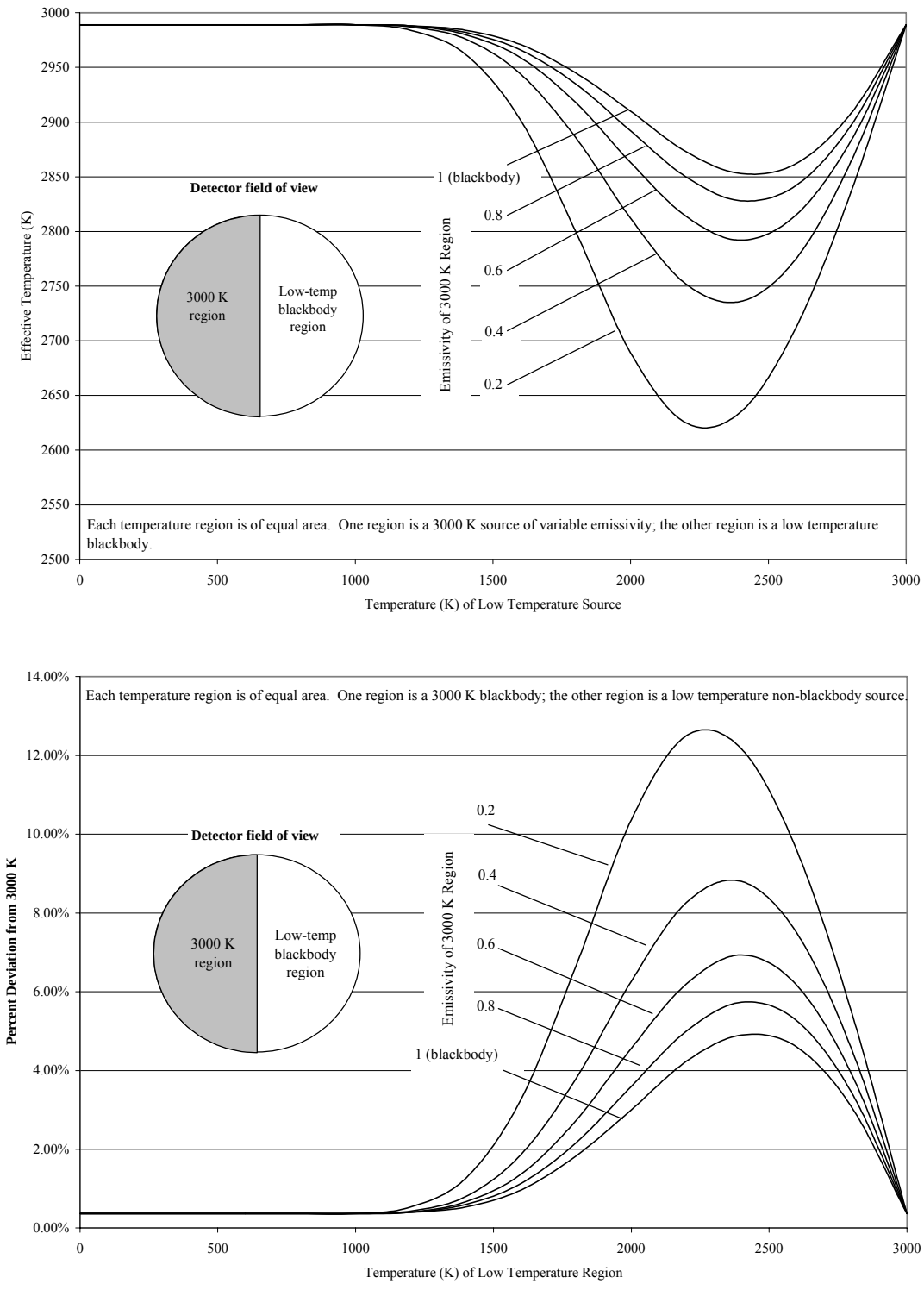

Figure 4.20: Effective spectrometric temperatures from dual-temperature source, 2 3000 K source of various emissivities and lower temperature blackbody region

4.4.3.2 Temporal averaging

The concepts illustrated above, for spatial averaging considerations, apply equally well to temporal averaging. Suppose that, rather than a temperature field with multiple temperatures in space, as shown in the previous section, that the temperature of the field varies during the time the spectrometer collects signal for one spectrum. In effect, this is no different from a field of view with spatial variations in temperature. Consider a temperature source of about 3000 K that passes through the spectrometer's field of view in some fraction of the integration time (the amount of time the spectrometer collects optical signal before generating a representation of the spectrum). If the spectrometer is exposed to room temperature (300 K) for the rest of the integration time, the exposure to the lower temperature will have a negligible effect on the spectrum. As discussed previously, this is due to the significant difference in the shapes of the spectra for low and high temperatures. In either space or time, low temperature spectra have little effect on the shape of high-temperature spectra.

5 Conclusion and recommendations

A number of significant findings have been discovered and explored in this study. An investigation into cost-effective methods of grinding MgO-doped Partially Stabilized Zirconia (PSZ) has revealed that dense vitreous bond SiC (Silicon Carbide) wheels exhibit unexpectedly good grinding performance. This prompted a study of mechanisms in the grinding of MgO-PSZ, including the flash temperatures generated. The translucence of MgO-PSZ in the visible and near-infrared ranges made it possible to observe heat generation during the grinding process. This involved collecting and analyzing the optical signal emitted by the hot process. Observing the grinding process through the workpiece also enabled the use of coolant in a grinding temperature study. Of various methods used, the spectrometric method provided the most dependable temperature indications. It offers a number of advantages over single- and dual-wavelength methods. The need to know the source emissivity, common in single-wavelength methods, is alleviated by a constant emissivity (i.e., graybody) assumption. The ability to detect luminescent peaks and the significantly greater number of data points give the spectrometer method advantage over dual-wavelength methods. Furthermore, since it is a multiple-wavelength method, spatial and temporal averaging are nearly negligible when the temperature difference is great. In such a case, the indicated temperature very nearly represents the highest temperature in the field of view.

This study has revealed a number of avenues for further investigation. While the possibilities for analyzing the causes and results of temperature generation are unlimited, four areas of investigation are suggested here. They provide opportunities to validate the

temperature indications of the current research, further develop the imaging and high-speed methods still needing refinement, and implement all of these methods in grinding temperature studies.

Perhaps the most intriguing possibility immediately is the comparison of the empirical flash temperature indications given here with results from the analytical models derived by many researchers. These analytical models may validate the results of this investigation, or it may be found that the flash temperature measured does not match the predicted values. In such a case, further insight into temperature generation and improvement of the measurement method will be gained. On the other hand, such a discrepancy may indicate that mechanisms of heat generation not considered in the models are at work. (Recall that Chandra and Rathore , 1995 cite a study by Meyer et al., 1970 reporting crack propagation temperatures of thousands of degrees Kelvin). All such possibilities should be investigated in the validation of this study's temperature indications.

Another possibility for validation and further investigation is the development of the imaging method. Due to its numerous benefits, it is recommended that a dual-color imaging camera be used. Thereby, spatial distributions of temperature, as well as absolute temperature values across the grinding zone, may be determined. Such a method would exhibit the benefits of multiple-wavelength methods for measuring flash temperature. The system may require development, but would provide valuable insights.

Similarly, improvement of the high-speed dual-wavelength method would provide numerous opportunities for research into the fundamentals of heat generation in grinding.

The increased temporal resolution it provides, combined with high spatial resolution, would enable analysis of the temperature generation due to individual abrasive grits. Such a method may be the first to examine heat generation from individual grits during their interaction with the workpiece.

Finally, it is recommended that all of the above methods be used to examine a larger number of wheel/workpiece combinations. The limited number of variations used provide some indication of the temperature generation mechanism, but more data would be very valuable.

The possibilities are extensive for fundamental studies involving temperature measurement through the workpiece in machining processes. This fundamental research may contribute to more cost effective machining processes by reducing workpiece burn, revealing the role of temperature in grinding performance, and indicating efficient cooling methods, among other improvements. The potential impact of such improvements indicates a strong possibility for continued development of machining temperature measurement methods.

References

Bifano, T. G.; Dow, T. A.; Scattergood, R. O. (1991) "Ductile regime grinding. A new technology for machining brittle materials" *J-Eng-Ind-Trans-ASME* vol 113, no 2, May 1991, 184-189

Chandra, B. P. and A. S. Rathore (1995) "Classification of mechanoluminescence" *Crystal Research Technology* 30, 7, 1995, 885-896

Chandrasekar, S., T. N. Farris, and B. Bhushan (1990) "Grinding temperatures for magnetic ceramics and steel" *Journal of Tribology* vol 112, Jul 1990, 535-541

Costa, H. L., V. C. Pandolfelli, and J. D. Biasoli de Mello (1997) "On the abrasive wear of zirconias" *Wear* 203-204, 626-636

Des Ruisseaux, N. R. and R. D. Zerkle (1970) "Thermal Analysis of the Grinding Process" *Journal of Engineering for Industry*, 92, May 1970, 428-434

DeWitt, D. P. and Gene D. Nutter (1988) Theory and Practice of Radiation Thermometry John Wiley and Sons, Inc.

Farris, T. N. and S. Chandrasekar (1990) "High-speed sliding indentation of ceramics: thermal effects" *Journal of Materials Science* vol 25, 4047-4053

Garvie, Ronald C. and Patrick S. Nicholson (1972) "Phase analysis in zirconia systems" *Journal of the American Ceramic Society* vol 55, no 6, 303-305

Gary, R. (1999) *Private communication*, Milacron Inc.

Griffioen, J. A., S. Bair, and W. O. Winer (1985) Global Studies of Mechanisms and Local Analyses of Surface Distress Phenomona., Institut National des Sciences Appliquees, Lyon, France, 3-6 Sept. 1985

Guo, C. and S. Malkin, (1994) "Analytical and experimental investigation of burnout in creep-feed grinding" *Annals of the CIRP* 43, 283-286

Guo, C. and S. Malkin (1995) "Analysis of energy partition in grinding" *Journal of Engineering for Industry* vol 117, Feb. 1995, 55-61

Hahn, R. S. (1956) "The relation between grinding conditions and thermal damage in the workpiece" *Trans ASME* 78, 807-812

Hebbar, R., S. Chandrasekar, and T. N. Farris (1992) "Ceramic grinding temperatures" *Journal of the American Ceramic Society* vol 75, no 10, 2742-2748

Incropera, F. and D. DeWitt (1996) Introduction to Heat Transfer, 3rd ed., John Wiley and Sons, Inc., 596-649

Jaeger, J. C. (1942) "Moving sources of heat and the temperature at sliding contacts" *Proceedings of the Royal Society of New South Wales*, vol 76, 203-224

Jen, T. C. and A. S. Lavine (1995) "A variable heat flux model of heat transfer in grinding: model development" *Journal of Heat Transfer* vol 117, May 1995, 473-478

Jen, T. C. and A. S. Lavine (1996) "A variable heat flux model of heat transfer in grinding with boiling" *Journal of Heat Transfer* vol 118, May 1996, 463-470

Ju, Y., T.N. Farris, and S. Chandrasekar (1998) "Theoretical analysis of heat partition and temperatures in grinding" *Journal of Tribology* vol 120, Oct 1998, 789-794

Kannappan, S. and S. Malkin (1972) "Effects of grain size and operating parameters on the mechanics of grinding" *Journal of Engineering for Industry* vol 94, Aug 1972, 833-842

Kohli, S., C. Guo, S. Malkin (1995) "Energy partition to the workpiece for grinding with aluminum oxide and CBN abrasive wheels" *Journal of Engineering for Industry* vol 117, May 1995, 160-168

Konsztowicz, K. J., E. A. Payzant, and H. W. King. (1995) "Suppression of the phase-transformation of ZrO2 and PSZ in colloidally processed zirconia-alumina composites" *Journal of Materials Science Letters* vol 14, no 16, Aug 1995, 1135-1137

Kops, L., M. C. Shaw (1983) "Application of infrared radiation measurements in grinding studies" Proceedings of the 11th North American Manufacturing Research Conference

Lavine, A. S. (1988) "A simple model for convective cooling during the grinding process" *Journal of Engineering for Industry* vol 110, Feb. 1988, 1-6

Lavine, A. S. (1991) "Thermal aspects of grinding with CBN" *Annals of the CIRP* vol 40, Jan 1991, 343-345

Lavine, A. S. and T. C. Jen (1991) "Coupled heat transfer to workpiece, wheel, and fluid in grinding, and the occurrence of workpiece burn", *International Journal of Heat and Mass Transfer*, vol 34, no 4/5, pp 983-992

Lavine, A. S., S. Malkin, and T. C. Jen (1989) "Thermal aspects of grinding with CBN wheels" *Annals of the CIRP* 38/1, 557-560

Malkin (1968) "The attritious and fracture wear of grinding wheels", ScD thesis, MIT, 1968

Malkin, S. and R. B. Anderson (1974) "Thermal aspects of grinding, Part 1: Energy partition" *Journal of Engineering for Industry*, Nov 1974, 1177-1183

Malkin, S. (1974) "Thermal aspects of grinding, Part 2: Surface temperatures and workpiece burn" *Journal of Engineering for Industry*, Nov 1974, 1184-1191

Ng, Daniel and Gustave Fralick (1999) "Temperature measurement of ceramic materials using a multiwavelength pyrometer" National Aeronautics and Space Administration Lewis Research Center, NASA TM 1999-208850

Outwater, J. O. and M. C. Shaw (1952) "Surface temperatures in grinding" *Transactions of the ASME*, Jan 1952, 73-86

Ramanath, S. and M. C. Shaw (1988) "Abrasive grain temperature at the beginning of a cut in fine grinding", *Journal of Engineering for Industry* vol 110, Feb 1988, 15-18

Shih, A. J. and T.M. Yonushonis (2000) "High infeed rate method for grinding ceramic workpiece with silicon carbide grinding wheels" U. S. Patent 6030277, Issued Feb. 29, 2000

Stevens, R. (1986) Zirconia and Zirconia Ceramics, Magnesium Elektron Publication No. 113, magnesium Elektron Ltd., Manchester, U.K.

Swain, M. V. and R. H. J. Hannink (1989) "Metastability of the martensitic transformation in a 12 mol% ceria-zirconia alloy: II, Grinding studies" *Journal of the American Ceramic Society* vol 72, no 8, 1358-1364

Taylor, R., J. R. Brandon, and Paul Morrell (1992) "Microstructure, composition and property relationships of plasma-sprayed thermal barrier coatings" *Surface & Coatings Technology* vol 50, no 2, 141-149

Touloukian, Y. S. and D. P. DeWitt (1970) Thermophysical properties of matter: The TPRC Data Series. Vol 8, Thermal radiative properties: Non-metallic solids Thermophysical Properties Research Center, Purdue University

Ueda, T., A. Hosokawa, and A. Yamamoto (1985) "Studies on temperature of abrasive grains in grinding-Application of infrared radiation pyrometer", *Journal of Engineering for Industry*, vol 107, May 1985, 127-133

Ueda, T., K. Yamada, and T. Sugita (1992) “Measurement of grinding temperature of ceramics using infrared radiation pyrometer with optical fiber” *Journal of Engineering for Industry* vol 114, Aug 1992, 317-321

Zhu, B., C. Guo, J. E. Sunderland, S. Malkin (1995) “Energy Partition to the Workpiece for Grinding of Ceramics” *Annals of the International Institute for Production Engineering Research, Manufacturing Technology*, Enschede, Netherlands, 21-26 Aug 1995